NASA TECHNICAL MEMORANDUM

NASA TM X-3222

NASA TM X-3222

EFFECT OF ENTRY-LIP DESIGN ON AERODYNAMICS AND ACOUSTICS OF HIGH-THROAT-MACH-NUMBER INLETS FOR THE QUIET, CLEAN, SHORT-HAUL EXPERIMENTAL ENGINE

Brent A. Miller, Benjamin J. Dastoli, and Howard L. Wesoky

Lewis Research Center
Cleveland, Ohio 44135

NATIONAL AERONAUTICS AND SPACE ADMINISTRATION • WASHINGTON, D. C. • MAY 1975

1. Report No.	2. Government Accession No.	3. Recipient's Catalog No.
NASA TM X-3222		

4. Title and Subtitle	5. Report Date
EFFECT OF ENTRY-LIP DESIGN ON AERODYNAMICS AND ACOUSTICS OF HIGH-THROAT-MACH-NUMBER INLETS FOR THE QUIET, CLEAN, SHORT-HAUL EXPERIMENTAL ENGINE	May 1975
	6. Performing Organization Code
7. Author(s)	8. Performing Organization Report No.
Brent A. Miller, Benjamin J. Dastoli, and Howard L. Wesoky	E-8160
	10. Work Unit No.
9. Performing Organization Name and Address	505-03
Lewis Research Center National Aeronautics and Space Administration Cleveland, Ohio 44135	11. Contract or Grant No.
	13. Type of Report and Period Covered
12. Sponsoring Agency Name and Address	Technical Memorandum
National Aeronautics and Space Administration Washington, D.C. 20546	14. Sponsoring Agency Code

15. Supplementary Notes

16. Abstract

Results of scale model tests of high-throat-Mach-number inlets designed to suppress inlet-emitted engine machinery noise conducted in the Lewis 2.74- by 4.58-meter (9- by 15-ft) V/STOL wind tunnel are presented. A vacuum system was used to induce inlet airflow with a siren as a noise source. Inlet mass flow was 11.68 kilograms (25.75 lbm) per second at a throat Mach number of 0.79. The effect of entry-lip design (contraction ratio and diameter ratio) on inlet total-pressure recovery, steady-state pressure distortion, performance at high incidence angles, and noise suppression was determined. With proper entry-lip design, total-pressure recovery in excess of 0.988 could be obtained statically at an average throat Mach number of 0.79. Total-pressure distortion was 5 percent. The reduction in the siren tone sound pressure level transmitted through the inlet was 10 to 14 dB relative to that measured at throat Mach 0.6. Good inlet performance was also obtained to high incidence angles at free-stream velocities of 41 and 61 meters per second. At an incidence angle of 50°, a throat Mach number of 0.79, and a free-stream velocity of 41 meters per second, total-pressure recovery was 0.982 with a total-pressure distortion of 14 percent. At this condition the reduction in inlet-emitted siren tone sound pressure level was 23 decibels relative to that measured at 0.6 throat Mach number.

17. Key Words (Suggested by Author(s))

Inlet design
Inlet lip design
Sonic inlet
High Mach number inlet
Choked inlet
Wind tunnel tests

18. Distribution Statement

Unclassified - unlimited
STAR category 02 (rev.)

19. Security Classif. (of this report)	20. Security Classif. (of this page)	21. No. of Pages	22. Price*
Unclassified	Unclassified	44	$3.75

* For sale by the National Technical Information Service, Springfield, Virginia 22151

EFFECT OF ENTRY-LIP DESIGN ON AERODYNAMICS AND ACOUSTICS OF HIGH-THROAT-MACH-NUMBER INLETS FOR THE QUIET, CLEAN, SHORT-HAUL EXPERIMENTAL ENGINE

by Brent A. Miller, Benjamin J. Dastoli, and Howard L. Wesoky

Lewis Research Center

SUMMARY

Scale model tests of high-throat-Mach-number inlets designed to suppress inlet-emitted engine machinery noise were conducted in the Lewis 2.75- by 4.58-meter (9- by 15-ft) V/STOL wind tunnel. The tests were conducted to support the development of a quiet, clean, short-haul experimental engine (QCSEE). The effect of entry-lip design on inlet total-pressure recovery, steady-state total-pressure distortion, performance at high incidence angles, and noise suppression was determined. Four entry lips were tested. Three had external forebody diameter ratios of 0.905 and internal area contraction ratios of 1.37, 1.46, and 1.56. The fourth had an external forebody diameter ratio of 0.935 and a contraction ratio of 1.46.

At static conditions the two entry lips having a diameter ratio of 0.905 and contraction ratios of 1.46 and 1.56 generally showed the better performances. At 0.79 throat Mach number, these entry lips produced a pressure recovery in excess of 0.988. Total-pressure distortion was approximately 5 percent. The noise transmitted through the inlet was reduced 10 to 14 decibels from the value at a throat Mach number of 0.6.

The entry lips with contraction ratios of 1.46 and 1.56 and diameter ratio of 0.905 showed the best performance when subjected to an 18-meter-per-second (35-knot) 90° crosswind. At these conditions separation-free operation was obtained over a wide range of average throat Mach numbers. These two entry lips also operated free from large-scale flow separations at incidence angles in excess of 60°, at a free-stream velocity of 41 meters per second (80 knots) and a throat Mach number of 0.79. At a 50° incidence angle, a 0.79 throat Mach number and a 41-meter-per-second (80-knot) free-stream velocity, these entry lips produced a sound pressure level reduction of approximately 23 decibels relative to that measured at throat Mach number of 0.6. The corresponding total-pressure recovery was 0.982 with a total-pressure distortion of approximately 14 percent.

INTRODUCTION

Lewis Research Center and the General Electric Co., as primary contractor, are developing the technology for a quiet, clean, short-haul, experimental engine (the QCSEE engine). Such an engine, intended for application to short takeoff and landing (STOL) aircraft, requires a close integration of the engine and its nacelle. The QCSEE inlet, which is an important part of the nacelle, is the subject of this report.

Two major factors contribute to making the inlet design more difficult for the QCSEE application than for conventional subsonic engines: the low noise goal set for the aircraft that will use the QCSEE engine (ref. 1) and the large upwash angles generated by STOL aircraft takeoff and landing operations (ref. 2).

An appreciable reduction in inlet-emitted engine machinery noise must be made to enable a four-engine aircraft to meet a noise goal of 95 effective perceived noise decibels (EPNdB) along a 152-meter (500-ft) sideline. Numerous investigations (refs. 3 to 8) have demonstrated that reductions in inlet-emitted engine noise can be achieved by increasing the inlet average throat Mach number above the values typically used with conventional inlets. A high-throat-Mach-number inlet was, therefore, selected for QCSEE. A design throat Mach number of 0.79 was tentatively selected to be representative of this type of inlet (refs. 6 to 8). This compares with 0.6 to 0.7 for conventional subsonic inlets.

The large upwash angles generated by the high wing-lift coefficients characteristic of STOL aircraft operations are of concern to the inlet designer. Typical low-speed conditions at which the QCSEE inlets will be judged are static conditions, a 90° crosswind at 18 meters per second (35 knots), and a 50° incidence angle at 41 meters per second (80 knots). Reference 9 indicates that inlet performance at low forward speeds, especially at high incidence angles, is strongly affected by inlet entry-lip design. Penalties for unsatisfactory entry-lip design are a loss in engine thrust and stall margin, with possible increased engine noise generation (ref. 10) and vibration. The results presented in reference 11 indicate that entry-lip design also significantly affects the acoustic suppression properties of high-throat-Mach-number inlets. A properly designed entry lip is thus essential.

The task of designing an inlet capable of operating satisfactorily at the high throat Mach numbers required for engine noise suppression while immersed in the high upwash flow characteristic of short-haul operation is difficult. An analytical study of proposed inlets for the QCSEE application (ref. 12) indicated that high surface Mach numbers and strong adverse pressure gradients would be encountered on the inlet entry lip at the QCSEE low-speed operating conditions. No experimental data could be found for inlets designed to operate at these conditions.

The purpose of the present investigation was to determine experimentally the effect of entry-lip design on the low-speed performance of the high-throat-Mach-number inlet

proposed for QCSEE. The inlets selected for testing were designed jointly by General Electric Co., Douglas Aircraft Company (a subcontractor), and Lewis Research Center personnel. The scale model inlets were then tested in a 2.74- by 4.58-meter (9- by 15-ft) V/STOL wind tunnel at Lewis. Measurements were made to determine inlet total-pressure recovery, steady-state total-pressure distortion, incidence angle at flow separation, and inlet-emitted noise. Two major entry-lip geometric variables were investigated: the internal lip area contraction ratio and the external forebody diameter ratio. Three of the entry lips tested had internal lip contraction ratios of 1.37, 1.46, and 1.56. The external forebody diameter ratio of these lips was 0.905. The effect of the external forebody diameter ratio was investigated with a fourth entry lip where the ratio was 0.935. The contraction ratio of this entry lip was 1.46.

The four entry lips were tested with the same inlet centerbody and diffuser. The diffuser-exit diameter was 30.48 centimeters (12 in.). The tests were conducted without a fan by using a vacuum system and the appropriate valves and controls to induce inlet airflow. A siren was used to simulate engine machinery noise so that the noise suppression properties of the inlets could be determined. The inlets were tested at tunnel airflow velocities of 0, 18, 41, and 61 meters per second (0, 35, 80, and 120 knots) at incidence angles of 0° to 90°. Inlet average throat Mach number was varied over a wide range both above and below the design value of 0.79.

SYMBOLS

a	major axis of internal lip (fig. 4)
b	minor axis of internal lip (fig. 4)
D	diameter
$\mathscr{D}_{max}$	inlet total-pressure distortion parameter, [(maximum total pressure) - (minimum total pressure)]/(average total pressure)
L	axial length of inlet (fig. 3)
$\overline{M}_t$	one-dimensional average throat Mach number
P	total pressure
p	static pressure
SPL	sound pressure level, dB
$\Delta(SPL)_{BPF}$	reduction in one-third-octave band sound pressure level at siren blade passing frequency, dB
V	velocity, m/sec (knots)
x	axial distance from inlet highlight (fig. 3)

Y external forebody thickness (fig. 4(a))

α incidence angle (angle between free-stream velocity and inlet centerline), deg

θ_m diffuser maximum local wall angle (fig. 3), deg

χ external forebody length (fig. 4(a))

ψ inlet circumferential position, deg

Subscripts:

c centerbody

d diffuser

e diffuser exit

hℓ highlight

m inlet maximum

t throat

0 free stream

1 rake measuring plane

APPARATUS AND PROCEDURE

Test Facility

Inlet tests were conducted in a 2.74- by 4.58-meter (9- by 15-ft) V/STOL wind tunnel (ref. 13). A vacuum system was used in place of a fan or compressor to induce inlet flow. A schematic view of the test installation and facility is shown in figure 1.

A venturi, calibrated in place against a standard ASME bellmouth that had been corrected for boundary-layer growth, was used to measure inlet airflow. The scatter in the airflow calibration data was approximately ±0.2 percent at the design inlet mass flow of 11.68 kilograms per second (25.75 lbm/sec). Inlet airflow was remotely varied using two butterfly valves arranged to give both course and fine adjustment. Inlet incidence angle was also remotely varied by mounting the test apparatus on a turntable. A swivel joint, containing a low-leakage-pressure seal, provided 360° rotation capability.

To determine the acoustic suppression properties of the inlet using the vacuum flow system a siren was installed in the duct downstream of the inlet. The siren was a 13.97-centimeter (5.5-in.) diameter single-stage fan modified by the addition of struts and a screen just upstream of the rotor to increase its noise level. The siren was located appproximately three inlet diameters downstream of the simulated fan face (fig. 1). Figure 1 also shows the microphones located in the wind tunnel approximately 20 meters

upstream of the test section. The microphones were used to measure the siren noise transmitted through the inlet. A photograph of the model, as it appeared in the wind-tunnel test section, is shown in figure 2.

Inlet Design

The major variables defining inlet design are shown in figure 3. The inlets tested had a diffuser-exit diameter D_e (equivalent to the fan diameter) of 30.48 centimeters and a throat diameter D_t of 25.31 centimeters. At the model design throat Mach number of 0.79, inlet airflow was 11.68 kilograms per second.

In keeping with the major objective of the test program (i.e., the selection of an inlet entry lip to permit high incidence angle operation) the inlets were fabricated in three parts, allowing replacement of the entry lip. The three parts are the removable entry lip, the diffuser, and the nonrotating centerbody. Four entry lips, one diffuser, and one centerbody were tested.

The variations in entry-lip design tested are shown schematically in figure 4. Figure 4(a) shows the dimensions used to define the external forebody and internal lip proportions. Two major entry-lip geometric variables were investigated: the internal lip area contraction ratio $(D_{h\ell}/D_t)^2$ and the external forebody diameter ratio $D_{h\ell}/D_m$. All entry lips were designed for cruise Mach numbers of approximately 0.7. Three of the entry lips tested, designated by the numbers 1, 2, and 3, had respective internal lip area contraction ratios of 1.37, 1.46, and 1.56. The external forebody diameter ratio for these entry lips was 0.905 with a forebody length to maximum diameter χ/D_m of 0.2. These three entry lips are shown in figure 4(b). A fourth entry lip, number 4, had a diameter ratio of 0.935 and a contraction ratio of 1.46. The external forebody length of this entry lip was 0.175 times its maximum diameter. This entry lip is compared with entry lip 2 in figure 4(c).

A summary of the inlets tested is presented in table I. Note that all entry lips have an elliptical internal lip contour but that the external forebody contours are not the same. Entry lips 1 to 3 have an external forebody contour defined by the DAC-1 (table I) thickness distribution.

The NACA-1 shape was used for entry lip 4 (ref. 14). The DAC-1 contour is more blunt near the highlight than the NACA-1 shape. The diffuser contour is defined by a cubic equation with a slope parallel to the inlet centerline at the throat and diffuser exit. The maximum local wall angle of 8.7° occurs at the midpoint of the diffuser.

Instrumentation and Data Reduction

Aerodynamic data. - The location and extent of inlet steady static-pressure instrumentation is shown in figure 5. Two axial rows of 20 static pressure taps each were located on the inlet extending from just outside the highlight to the rake measuring plane. One row was located on the windward ($\psi = 0$) side of the inlet and the other was located on the leeward ($\psi = 180^{\circ}$) side. As shown in sections AA and BB of figure 5, one circumferential ring of eight static-pressure taps was located at the throat and another just upstream of the rake measuring plane. Section CC shows the total-pressure rakes and static-pressure taps located at the rake measuring plane. This is the approximate axial position that would normally lie in the plane of the fan face. Rake plane total-pressure measurements were made using both hub and tip boundary-layer rakes as well as total-pressure rakes spanning the entire annulus. Eight full-span total-pressure rakes were used with six equal-area-weighted tubes per rake. The hub and tip boundary-layer rakes each contained five total-pressure measurements.

Inlet total-pressure recovery P_1/P_0 was computed using all measured total pressures, including boundary-layer rakes, with the appropriate area weighting terms. However, in computing inlet total-pressure distortion $\mathscr{D}_{max}$, boundary-layer measurements taken closer to the wall than the nearest tube on the six-element equal-area-weighted rakes were omitted. Using these rakes as a reference results in excluding those measurements closer to the wall than 8.3 percent of the annulus area.

Inlet average throat Mach number $\overline{M}_t$ was computed using the inlet flow measured by the venturi with a correction made for the high-pressure air required to drive the siren. One-dimensional flow was assumed for computing the Mach number using the inlet geometric throat area. The inlet airflow was corrected to standard conditions.

Acoustic data. - Noise data were taken with four microphones located in the wind-tunnel settling chamber upstream of the test section (fig. 1). The hard walls of the wind tunnel approximate a reverberant chamber and eliminate any directional noise variation due to changing incidence angle. The microphone outputs were recorded on magnetic tape and then processed with a one-third-octave band analyzer.

Figure 6 shows a narrow-band analysis of a typical noise spectra measured with a microphone. The upper curve shows the spectrum measured with both the siren and wind tunnel in operation. Inlet average throat Mach number is 0.6 where little or no inlet noise suppression occurs. The bottom curve shows wind-tunnel noise with the siren turned off. Data for both curves were taken at a free-stream velocity V_0 of 41 meters per second (80 knots). The large spike appearing in the siren spectrum occurs at the siren rotor-blade passing frequency. A blade passing frequency of 8000 hertz was selected by scaling the QCSEE fan to this model size. Fan face diameter was used as the scaling factor.

Noise data are presented in all subsequent figures for the one-third-octave band containing the 8000-hertz spike. These data are shown in terms of the noise reduction parameter $\Delta(SPL)_{BPF}$, where $\Delta(SPL)_{BPF}$ is the reduction in siren tone sound pressure level measured as the average throat Mach number is increased above 0.6. A correction of approximately 1.5 decibels was made in the siren source noise to account for convective flow effects within the duct as inlet weight flow was increased to the maximum value. A throat Mach number of 0.6 was selected to be representative of conventional inlets where no appreciable fan or compressor noise reduction due to throat Mach number is observed. According to this definition the maximum detectable noise reduction is approximately equal to the difference between the siren blade passing spike at a throat Mach 0.6 and the tunnel background noise level.

Test Procedure

The inlets were tested at free-stream velocities of 0, 18, 41, and 61 meters per second (0, 35, 80, and 120 knots) and at incidence angles of 0 to 90°. Airflow was varied from that producing an average inlet throat Mach number of approximately 0.15 to the maximum value that could be passed by the inlet.

Tests were conducted at a free-stream velocity of 18 meters per second (35 knots) and 90° incidence angle to simulate crosswinds during engine startup and ground taxi. These tests were conducted by first setting tunnel velocity and then positioning the model at a 90° incidence angle. The model remained in this position, and data were taken as the inlet flow was increased from zero to the maximum value. Aerodynamic and acoustic data were taken simultaneously for this and all other test conditions.

Data were recorded at a free-stream velocity of 41 meters per second (80 knots) to approximate the takeoff and approach velocity of short-haul or STOL type of aircraft. A velocity of 61 meters per second (120 knots) was included to be representative of CTOL takeoff and landing operations.

The data recorded to define the incidence angle at entry-lip flow separation and reattachment were obtained by first setting tunnel velocity and inlet airflow. Data were then recorded in real time as the incidence angle was increased from zero at approximately 2° per second. The data recorded at discrete angles were obtained by setting tunnel velocity and inlet weight flow while at a zero incidence angle. Data were then recorded, and the incidence angle was increased to the next value. Data were again recorded and the procedure repeated.

RESULTS AND DISCUSSION

Inlet total-pressure recovery P_1/P_0 total-pressure distortion $\mathscr{D}_{max}$ and sound pressure level reduction are presented as a function of average throat Mach number for each inlet tested. Selected data were cross-plotted to illustrate how the aerodynamic and acoustic performances are affected by entry-lip design, incidence angle, and free-stream velocity. Several representative data points were selected to illustrate how inlet axial static-pressure distributions and rake plane total-pressure contours were affected by model operating conditions. The incidence angles producing entry-lip flow separation and reattachment are shown as a function of average throat Mach number and free-stream velocity for each entry lip.

Performance at Static Conditions

Figure 7 shows the pressure recovery, distortion, and sound pressure level reduction obtained statically with the four entry lips as functions of average throat Mach number. Tests were conducted to the maximum flow that could be passed by the inlets. However, because of inlet surface curvature and the resulting flow curvature and velocity gradients, the maximum flow that can be passed through the inlet throat is less than the theoretical value computed assuming one-dimensional Mach 1 flow. For this reason the computed average throat Mach number (which is obtained from a one-dimensional calculation using the throat area and the measured flow) is always less than one for all entry lips even though they may be passing maximum flow. Note that entry lip 3, with the highest contraction ratio and hence the lowest surface curvature, passes the maximum flow. The reduction in flow below that required to yield a computed average throat Mach number of 1 represents an inlet mass-flow coefficient analogous to a nozzle discharge coefficient.

At the design throat Mach number of 0.79, the total-pressure recovery ranged from approximately 0.975 to 0.99 with a distortion of between 5 and 10 percent (fig. 7). The lowest distortion (approx. 5 percent) and highest recovery (above 0.988) were measured with entry lips 2 and 3. The sound pressure level reduction was 10 to 14 decibels with these two entry lips at a throat Mach number of 0.79.

Figure 8 shows the relation between sound pressure level reduction and inlet aerodynamic performance obtained by cross-plotting the data of figure 7. The figure indicates that for a given value of sound pressure level reduction, better aerodynamic performance was generally obtained as inlet contraction ratio increased from 1.37 to 1.56. Entry lip 4, even though it has a contraction ratio of 1.46, did not perform as well as the others. This was attributed to its higher (0.935) external forebody diameter ratio. The diameter ratio of the other entry lips was 0.905. Entry lips 2 and 3, with contrac-

tion ratios of 1.46 and 1.56, generally yielded the highest recovery and lowest distortion for a given noise reduction of the four entry lips tested. The largest noise reduction (approx. 40 dB) was obtained with entry lip 4. However, this data point shows the poorest aerodynamic performance.

The type of rake plane total-pressure contours produced at static conditions are illustrated in figure 9 for entry lip 3. Figure 9(a) shows the drop that occurred in inlet surface static pressure as average throat Mach number was increased from 0.6 to 0.87. The horizontal dashed line indicates that supersonic surface velocities were measured for average throat Mach numbers above approximately 0.80. Figure 9(b) shows the resulting rake plane total-pressure contours measured at an average throat Mach number of 0.87. The high surface velocity near the inlet throat, as well as normal boundary-layer growth within the diffuser, generated the total-pressure losses shown.

Performance with an 18-Meter-per-Second (35-Knot) 90° Crosswind

Figure 10 shows the basic aerodynamic and acoustic performance obtained with an 18-meter-per-second (35-knot), 90° crosswind. Data were taken for each inlet starting at zero flow and progressing to the maximum value that could be passed through the inlet. Open symbols denote attached inlet flow, and solid symbols show those operating conditions resulting in entry-lip flow separation.

Figure 10 indicates that flow separation existed at average throat Mach numbers below approximately 0.3, with flow attachment occurring as inlet throat Mach number was increased. Entry lips 2 and 3 have the largest separation-free operating range. These two entry lips also produced the highest pressure recovery and lowest distortion of the four designs.

The noise and pressure data presented in figure 10 are cross-plotted in figure 11. Figure 11 shows that for a given desired sound pressure level reduction, entry lips 2 and 3 yield significantly better aerodynamic performance at crosswind conditions than the other lips.

The nature of the separated and attached flow conditions observed with the 90° crosswind are illustrated in figure 12. Data shown are for entry lip 3. Figure 12(a) shows the inlet axial static-pressure distribution measured on the windward side of the inlet with fully separated flow and the resulting total-pressure contours at the rake measuring plane. Note the flat static-pressure distribution extending from the inlet highlight to the diffuser exit. This flat profile is typical of those obtained when flow separation occurred near the highlight. The total-pressure contours indicate a region of total-pressure loss downstream of the windward lip.

Axial static-pressure distributions are shown in figure 12(b) for both the windward ($\psi = 0$) and leeward ($\psi = 180^{\circ}$) side of the inlet. Note that the 90° incidence angle pro-

duces higher surface velocities on the windward lip than on the leeward lip. However, the figure indicates attached flow with diffusion from supersonic velocities beginning just downstream of the throat. The resulting total-pressure contour indicates a small region of total-pressure loss downstream of the windward lip. The nonaxisymmetric nature of this pressure contour is not a result of inlet entry-lip flow separation. It is due to the high surface velocities and resulting boundary-layer growth within the inlet as a result of the 90° crosswind.

Performance at Simulated Takeoff and Landing Conditions

Two series of tests were conducted at simulated takeoff and landing conditions. The first series was conducted to determine the incidence angle producing inlet flow separation for each of the four entry lips. The incidence angle required to obtain flow reattachment was also determined. These tests resulted in defining an operating envelope free from incidence-angle induced flow separation for each entry lip as a function of average throat Mach number and free-stream velocity. The second test series was conducted to determine in detail inlet aerodynamic and acoustic performance within this operating envelope. Data were also obtained outside the envelope to assess the severity of entry-lip flow separation and its effect on inlet performance.

Inlet incidence angle at entry-lip flow separation. - Figure 13 indicates how flow separation and reattachment were identified using inlet steady-state surface static-pressure measurements as well as the total-pressure measurements taken at the rake plane. The data shown are for entry lip 2 operating at a free-stream velocity of 41 meters per second (80 knots). The solid line on figure 13(a) shows the reduction in lip surface static pressure that occurs as incidence angle is increased. The pressure was measured on the windward side of the inlet approximately midway between the highlight and the throat. As incidence angle was increased to approximately 69°, flow separation occurred and the resulting abrupt increase in static pressure is easily identified. Flow reattachment, shown by the dashed line, was identified in a similar manner by gradually reducing incidence angle until the lip static-pressure measurement indicated flow reattachment.

The validity of using just a single static-pressure measurement to define entry-lip flow separation or reattachment is verified by the inlet axial static-pressure distributions and total-pressure contour plot shown in figure 13(b). Axial static-pressure distributions are shown for both attached and separated flow. The respective incidence angles are 63° and 70°. The relative flatness of the distribution shown at an incidence angle of 70° indicates that flow separation has occurred well forward on the entry lip. The total-pressure contour plot shows that this flow separation occurred on the windward ($\psi = 0$) side of the inlet resulting in large total-pressure losses.

Basic aerodynamic and acoustic data. - Figures 16 to 19 show the total-pressure recovery, distortion, and sound pressure level reduction obtained with each entry lip as a function of average throat Mach number and incidence angle at free-stream velocities of 41 and 61 meters per second (80 and 120 knots). Open symbols denote those operating conditions resulting in attached inlet flow, and solid symbols denote those conditions resulting in entry-lip flow separation. Dashed lines are used to indicate those data points showing a large change in inlet performance. The crosshatched band on the sound pressure level plot shows the limiting detectable noise reduction. This was determined by the acoustic characteristics of the test facility. The limiting detectable noise reduction at a free-stream velocity of 41 meters per second (80 knots) is approximately equal to the difference between the siren blade passing spike and the tunnel background noise (fig. 6).

Those data points indicating attached flow (figs. 16 to 19) show a general trend toward lower pressure recovery and higher distortion as average throat Mach number and incidence angle are increased. However, several of these data points show an abrupt deterioration in aerodynamic performance at high average throat Mach numbers. This can be illustrated with entry lip 2 when operating at a zero incidence angle and a 61-meter-per-second (120-knot) free-stream velocity. An abrupt drop in pressure recovery occurs at an average throat Mach number of approximately 0.87 (points A and B in fig. 17(b)). These data points were analyzed in more detail in an attempt to explain this behavior.

Figure 20 shows the inlet axial static-pressure distributions measured at these two points. Also shown in the figure are the measured values of average throat Mach number and rake-plane static-pressure to free-stream total-pressure ratio. This pressure ratio is an indication of the amount of suction applied to the inlet. The figure indicates that for both cases the surface velocity becomes supersonic at approximately the midpoint on the entry lip. For data point A the region of supersonic flow extends to just downstream of the throat plane. But for data point B the region of supersonic flow extends well downstream of the throat plane into the diffuser. Although the rake plane static pressure was reduced in going from point A to point B, the average throat Mach number, and hence inlet weight flow, remained nearly constant. This indicates that limiting flow was reached at point A with no further increase possible. The inlet appears to be behaving somewhat like a Laval nozzle as the downstream pressure is reduced, with a shock-boundary-layer interaction process believed responsible for the loss in inlet performance. Note that this loss in inlet performance is a result of a different phenomenon than the entry-lip separation defined in figures 13 to 15. The static-pressure distribution of figure 20 indicates attached flow.

The reduction in sound pressure level shown in figures 16 to 19 indicates that noise reduction generally increases with increasing average throat Mach number. For entry

The incidence angles resulting in entry-lip flow separation, obtained by increasing the incidence angle at constant average throat Mach number to the point of separation, are shown in figure 14. The separation angle is plotted against the average throat Mach number measured just before separation for two values of free-stream velocity. The separation angles are shown as bands to indicate the degree of nonrepeatability of the data due to the unsteady nature of flow separation. Entry-lip flow is attached at incidence angles below the band and fully separated at angles above the band. Within the band incipient, partial or total flow separation may exit.

Figure 14(a) shows that the objective of obtaining separation-free operation up to a 50° incidence angle at an average throat Mach number of 0.79 and free-stream velocity of 41 meters per second (80 knots) was easily met by entry lips 2 and 3. Both operated separation free to in excess of 60° at this condition. Entry lip 4, with the highest external forebody diameter ratio, and lip 1, with the lowest contraction ratio, showed the poorest performance, with separations at approximately 33° and 43°, respectively. This figure also shows that for each entry lip the separation angle increases with average throat Mach number to a maximum value and then decreases with further increases in Mach number. An examination of inlet axial static-pressure distributions and rake plane boundary-layer profiles indicates that this behavior may be attributable to the appearance of shock-boundary-layer interactions as average throat Mach number is increased.

Flow separation results in an abrupt drop in inlet weight flow and, hence, average throat Mach number. This is indicated by the data of figure 15, where the incidence angles resulting in flow reattachment, obtained by reducing incidence angle from the region of separated flow to the point of flow reattachment, are plotted against average throat Mach number. However, the Mach number plotted here is that measured with separated flow just before flow reattachment. Note that the maximum Mach number obtainable with flow separation (fig. 15) was approximately 0.68, compared with approximately Mach 0.86 obtained with attached flow.

The incidence angle at flow reattachment, shown in figure 15(a) for a free-stream velocity of 41 meters per second (80 knots), is highest for entry lips 2 and 3 and lowest for entry lip 4. Some hysteresis can be detected by comparing figures 14(a) and 15(a): at a constant throat Mach number the angle of flow reattachment is generally lower than the angle of flow separation. This is also evident in the lip static-pressure measurements shown in figure 13(a).

The separation bounds of figure 14(b) indicates that entry lip 3 performs significantly better than the others at a free-stream velocity of 61 meters per second (120 knots). At an average throat Mach number of 0.79, separation-free operation was obtained to approximately 60° with this entry lip and to approximately 43° with entry lip 2. The incidence angle at flow reattachment for a free-stream velocity of 61 meters per second (120 knots) is shown in figure 15(b) for entry lips 1 and 2. Data were not recorded for entry lips 3 and 4.

lip 2 at a free-stream velocity of 61 meters per second (80 knots; fig. 17(b)), the peak noise suppression occurred at data point B.

For each inlet and at constant average throat Mach number, figures 16 to 19 indicate that increasing incidence angle tends to increase noise suppression. However, the maximum attainable throat Mach number and noise reduction occurred at a zero incidence angle. A general trend towards a lower maximum attainable throat Mach number and noise reduction can be detected as incidence angle is increased (e.g., see fig. 16(a)). The relation of sound pressure level reduction to inlet aerodynamic performance is presented in the next section as a function of entry-lip design, incidence angle, and free-stream velocity.

Comparison of Aerodynamic and Acoustic Performance

Figures 21 to 25 show inlet pressure recovery and distortion as functions of sound pressure level reduction. The data shown are crossplots or repeats of that presented in previous figures for those conditions where the average throat Mach number was greater than or equal to approximately 0.6. Data are not shown for those conditions resulting in entry-lip flow separation or excessive inlet performance losses at or near inlet limiting flow.

Figures 21 to 23 show the effect of entry-lip design on inlet performance at incidence angles of 0, 30°, and 50°. Performance obtained at a free-stream velocity of 41 meters per second (80 knots) is shown in parts (a) of these figures, and that obtained at 61 meters per second (120 knots) is presented in parts (b). At a zero incidence angle entry-lip design affects inlet performance much as it did at static conditions (see figs. 6 and 21); that is, those entry lips having the largest internal lip contraction ratio generally show the best performance. Entry lips 2 and 3 show maximum sound pressure level reductions of approximately 30 decibels at a free-stream velocity of 41 meters per second (80 knots) with a corresponding pressure recovery in excess of 98 percent and a distortion of less than 8 percent. Entry lips 1 and 4 show somewhat poorer aerodynamic performance for the same noise reduction.

With an increase in the free-stream velocity of 61 meters per second (120 knots, there is little effect of entry lip design on inlet operation (fig. 21(b)). This is attributed to the improvement in entry-lip aerodynamics that generally occurs with increased free-stream velocity (ref. 9). This effect is apparently strong enough at a free-stream velocity of 61 meters per second (120 knots) to overshadow performance differences caused by changes in entry-lip design. The highest noise reduction recorded for entry lip 2, before encountering large aerodynamic performance losses, was approximately 18 decibels (fig. 17(b)). A closer data point spacing in the vicinity of high average throat Mach number may have shown higher noise suppression before experiencing inlet

performance loss. Entry lips 1, 3, and 4 did, however, yield a 27-decibel noise reduction with a pressure recovery of approximately 0.983 and a distortion of about 7.5 percent. Note that entry lip 1 yielded the highest noise reduction, approximately 32 decibels.

At a 30° incidence angle entry-lip design has a significant effect on inlet performance at both free-stream velocities (fig. 22). Figure 22 indicates that increasing the incidence angle to 30° negates the improvement in entry-lip aerodynamics that were noted when free-stream velocity was increased from 41 to 61 meters per second (80 to 120 knots) at a zero incidence angle. Again, for a specified noise reduction, the entry lips having the larger internal lip contraction ratios generally exhibit the best aerodynamic performance.

The performance measured at 50° incidence angle is shown in figure 23. At a free-stream velocity of 41 meters per second (80 knots) (fig. 23(a)), entry lips 2 and 3 yield a maximum noise reduction of approximately 23 decibels. The total-pressure recovery at this point is 0.982 with a total-pressure distortion of approximately 14 percent. As was shown in figure 15(a), only entry lip 3 provided separation-free operation at a 50° incidence angle and 61-meter-per-second (120-knot) free-stream velocity. Therefore, data for only this inlet appears in figure 23(b).

The effect of incidence angle on inlet performance is shown in figure 24(a) for entry lip 2 and in figure 24(b) for entry lip 3. The free-stream velocity is 41 meters per second (80 knots). The figure indicates that, for a constant value of sound pressure level reduction, increasing the incidence angle from 0 to 50° produces a progressive drop in pressure recovery and a corresponding increase in distortion. Note also the progressive drop in the maximum attainable noise reduction with increasing incidence angle. However, at all incidence angles, noise reductions in excess of approximately 22 decibels were measured for both entry lips at both free-stream velocities.

The effect of free-stream velocity on inlet performance is shown in figure 25. Data are shown at a zero incidence angle for each entry lip at free-stream velocities of 0, 41, and 61 meters per second (0, 80, and 120 knots). All entry lips show an improvement in aerodynamic performance with increasing free-stream velocity. The maximum sound pressure level reduction obtained did not appear to be systematically affected by increasing free-stream velocity from 0 to 41 and finally to 61 meters per second (0 to 80 and to 120 knots).

A summary of the sound pressure level reduction obtained with each entry lip is presented in figure 26 for a free-stream velocity of 41 meters per second (80 knots). Data are shown for incidence angles of 0 and 30°. At the design throat Mach number of 0.79 entry lip 2 yields the largest noise reduction. However, all entry lips, except entry lip 4 at a 30° incidence angle, yield a maximum sound pressure level reduction in excess of 22 decibels.

SUMMARY OF RESULTS

The effect of entry lip design on the aerodynamic and acoustic performance of high throat Mach number inlets was investigated in a 2.74- by 4.58-meter (9- by 15-ft) V/STOL wind tunnel. The two major entry-lip geometric variables investigated were internal lip contraction ratio and external forebody diameter ratio. Some specific results of the tests are as follows:

1. At static conditions the two entry lips having a diameter ratio of 0.905 and contraction ratios of 1.46 and 1.56 generally yielded the highest total-pressure recovery and lowest distortion. At the model design throat Mach number of 0.79, these entry lips produced an inlet pressure recovery in excess of 0.988 with a total-pressure distortion of approximately 5 percent. The corresponding sound pressure level reduction was 10 to 14 decibels.

2. Tests with an 18-meter-per-second (35-knot) 90° crosswind indicated flow separation at average throat Mach numbers below approximately 0.3 with flow attachment occurring as throat Mach number was increased. The two entry lips having a diameter ratio of 0.905 and contraction ratios of 1.46 and 1.56 had the largest separation-free throat Mach number operating range. These two entry lips also produced the highest pressure recovery and lowest distortion of the four designs.

3. The two entry lips having a diameter ratio of 0.905 and contraction ratios of 1.46 and 1.56 met the objective of operating separation free to a 50° incidence angle at an average throat Mach number of 0.79 and free-stream velocity of 41 meters per second (80 knots). These entry lips operated free from large scale flow separations at incidence angles in excess of 60°. The entry lip having the high external forebody diameter ratio (0.935), showed the poorest performance, with flow separation occurring at approximately 33° incidence angle.

4. Increasing incidence angle at free-stream velocities of 41 and 61 meters per second (80 and 120 knots) produced a progressive drop in pressure recovery and a corresponding increase in distortion for all entry lips. The entry lips having a diameter ratio of 0.905 and contraction ratios of 1.46 and 1.56 showed the best performance at all incidence angles. At a 50° incidence angle and a 41-meter-per-second (80-knot) free-stream velocity, these entry lips produced a noise reduction of approximately 23 decibels. The corresponding total-pressure recovery was 0.982 with a total-pressure distortion of approximately 14 percent.

5. Inlet performance losses, attributed to a shock - boundary-layer interaction process, was observed in several instances at maximum (choked) weight flows. The resulting large changes in inlet aerodynamic performance could adversely affect engine operation and stability. An examination of the inlet axial static-pressure distributions

indicated that inlet behavior at maximum flow was similar to that observed with Laval nozzles when operated at downstream pressures lower than that required to reach limiting flow.

Lewis Research Center,
National Aeronautics and Space Administration,
Cleveland, Ohio, January 8, 1975,
505-03.

REFERENCES

1. Rabone, G. R.; Lee, R.; Chamay, A. J.; and Edkins, D. P.: QCSEE Task I. Parametric Study. General Electric Co., 1973.
2. Albers, James A.: Predicted Upwash Angles at Engine Inlets for STOL Aircraft. NASA TM X-2593, 1972.
3. Chestnutt, David: Noise Reduction by Means of Inlet-Guide-Vane Choking in an Axial-Flow Compressor. NASA TN D-4682, 1968.
4. Study and Development of Turbofan Nacelle Modifications to Minimize Fan-Compressor Noise Radiation. Volume V - Sonic Inlet Development. NASA CR-1715, 1971.
5. Lumsdaine, Edward: Development of a Sonic Inlet for Jet Aircraft. Inter-Noise 1972 Proceedings, Washington, D. C., Oct. 4-6, 1972, pp. 501-506.
6. Miller, Brent A.; and Abbott, John M.: Aerodynamic and Acoustic Performance of Two Choked-Flow Inlets Under Static Conditions. NASA TM X-2629, 1972.
7. Miller, Brent A.; and Abbott, John M.: Low-Speed Wind-Tunnel Investigation of the Aerodynamic and Acoustic Performance of a Translating-Centerbody Choked-Flow Inlet. NASA TM X-2773, 1973.
8. Klujber, F.: Results of an Experimental Program for the Development of Sonic Inlets for Turbofan Engines. AIAA Paper 73-222, Jan. 1973.
9. Albers, James A.; and Miller Brent A.: Effect of Subsonic Inlet Lip Geometry on Predicted Surface and Flow Mach Number Distributions. NASA TN D-7446, 1973.
10. Wesoky, Howard L.; Abbott, John M.; Albers, James A.; and Dietrich, Donald A.: Low-Speed Wind Tunnel Tests of a 50.8-Centimeter (20-in.) 1.15-Pressure-Ratio Fan Engine Model. NASA TM X-3062, 1974.

11. Groth, Harold W.: Sonic Inlet Noise Attenuation and Performance with a J-85 Turbojet Engine as a Noise Source. AIAA Paper 74-91, Jan. 1974.

12. Albers, James A.; Stockman, Norbert O.; and Hirn, John J.: Aerodynamic Analysis of Several High Throat Mach Number Inlets for the Quiet Clean Short-Haul Experimental Engine. NASA TM X-3183, 1974.

13. Yuska, Joseph A.; Diedrich, James H.; and Clough, Nestor: Lewis 9- by 15-Foot V/STOL Wind Tunnel. NASA TM X-2305, 1971.

14. Baals, Donald D.; Smith, Norman F.; and Wright, John B.: The Development and Application of High-Critical-Speed Nose Inlets. NACA Rep. 920, 1948.

TABLE I. - SUMMARY OF INLET GEOMETRIC VARIABLES

(a) Entry lip

Geometric variable	Entry-lip number			
	1	2	3	4
Internal lip contraction ratio, $(D_{h\ell}/D_t)^2$	1.37	1.46	1.56	1.46
External forebody diameter ratio, $D_{h\ell}/D_m$	0.905	0.905	0.905	0.935
Ratio of external forebody length to maximum diameter, χ/D_m	0.2	0.2	0.2	0.175
External forebody contour[a]	DAC-1	DAC-1	DAC-1	NACA-1
External forebody proportions, χ/Y	4.21	4.21	4.21	5.38
Internal lip contour	Ellipse	Ellipse	Ellipse	Ellipse
Internal lip proportions, a/b	2.0	2.0	2.0	2.0
Ratio of overall inlet length to diffuser exit diameter, L/D_e	0.97	1.00	1.03	1.00

(b) Diffuser

Ratio of exit flow area to inlet flow area, $(D_e^2 - D_c^2)/D_t^2$	1.21
Ratio of diffuser length to exit diameter, L_d/D_e	0.826
Ratio of centerbody diameter to diffuser exit diameter, D_c/D_e	0.400
Maximum local wall angle, θ_m, deg	8.7
Location of maximum local wall angle, percent L_d	50
Equivalent conical half angle, deg	2.9
Surface contour	Cubic

(c) Centerbody

Ratio of length to diameter, L_c/D_c	0.75
Surface contour	Ellipse
Ratio of centerbody length to diffuser length, L_c/L_d	0.357

[a]The DAC-1 contour was developed by the Douglas Aircraft Company and is given by

$$\left(\frac{y}{Y}\right)^2 = 2.318\left(\frac{x}{\chi}\right) - 2.748\left(\frac{x}{\chi}\right)^2 + 2.944\left(\frac{x}{\chi}\right)^3 - 1.113\left(\frac{x}{\chi}\right)^4$$

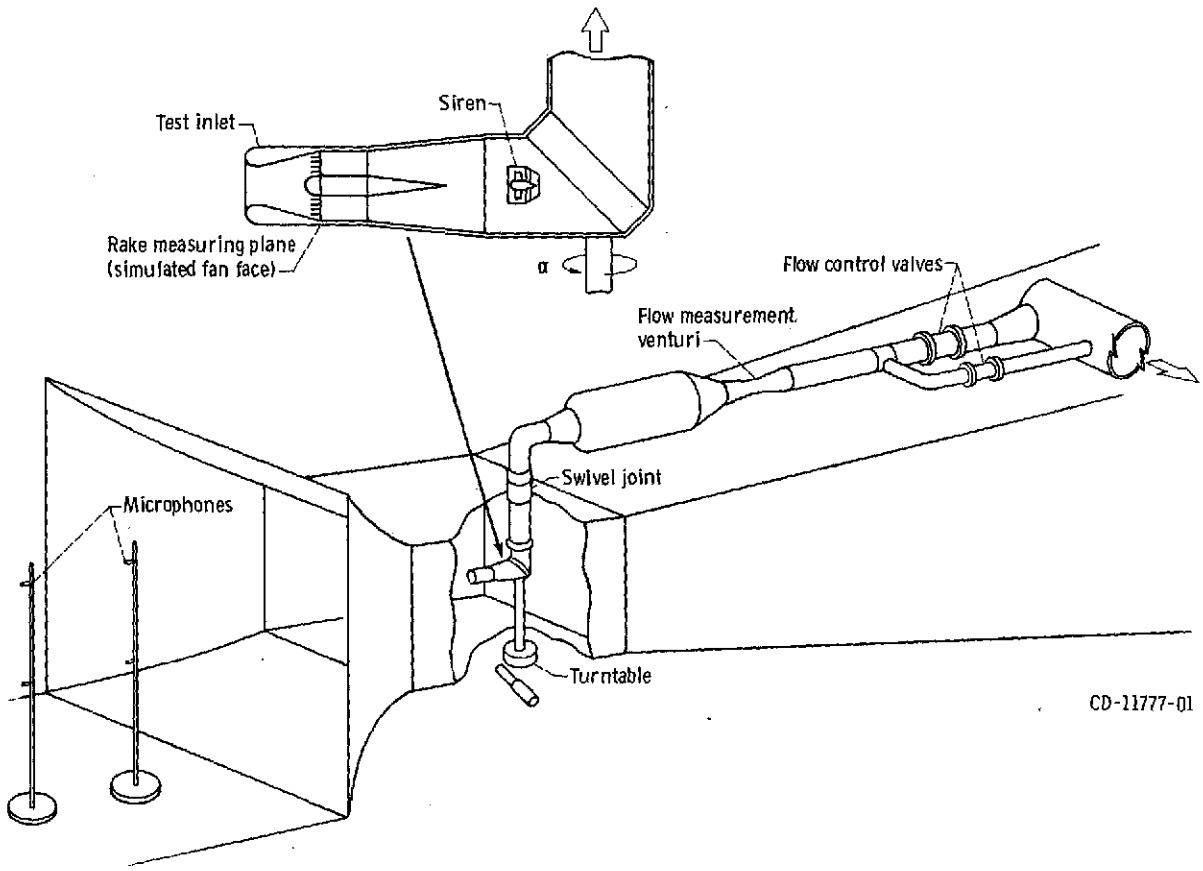

Figure 1. - V/STOL wind tunnel showing model arrangement and microphone locations.

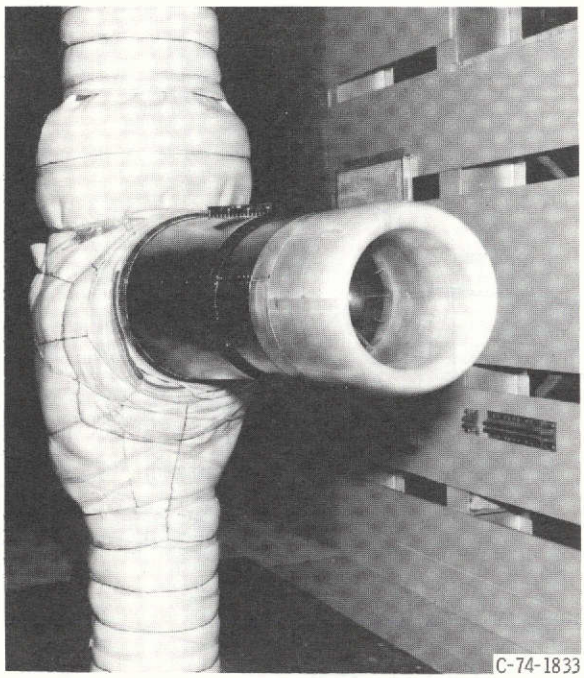

Figure 2. - Installation of model in V/STOL wind tunnel.

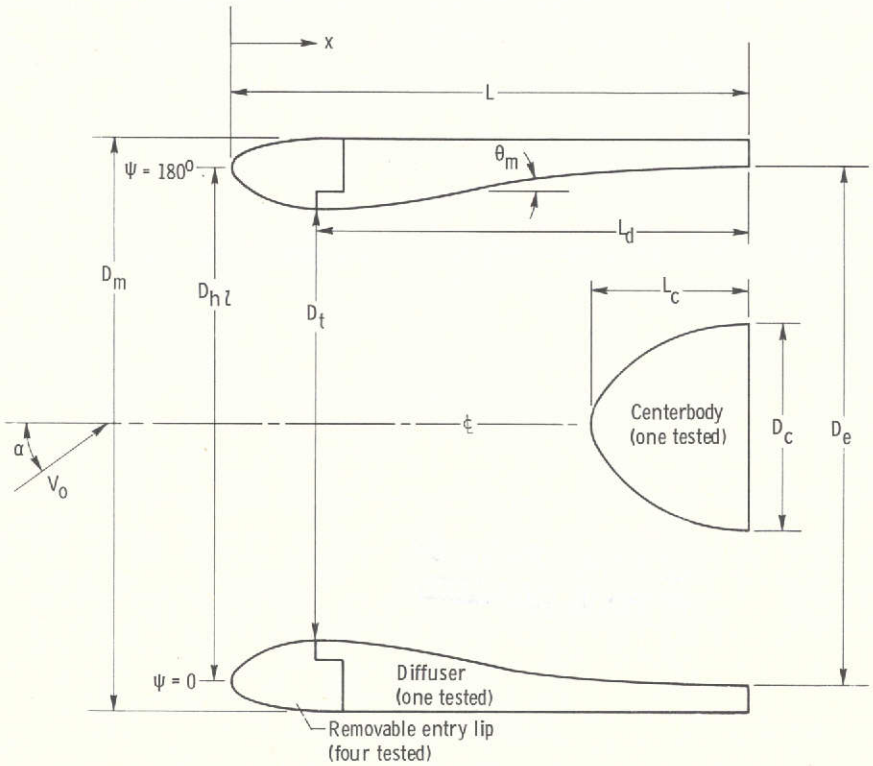

Figure 3. - Inlet nomenclature.

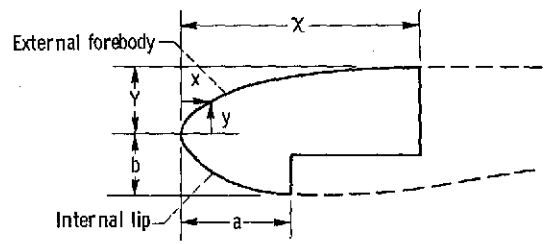

(a) Entry lip nomenclature.

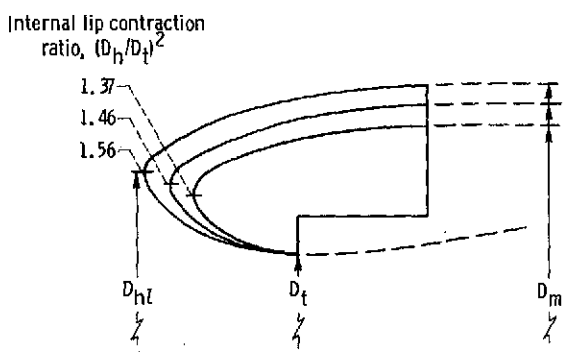

(b) Internal lip contraction ratios. External forebody diameter ratio, D_{hl}/D_m, 0.905.

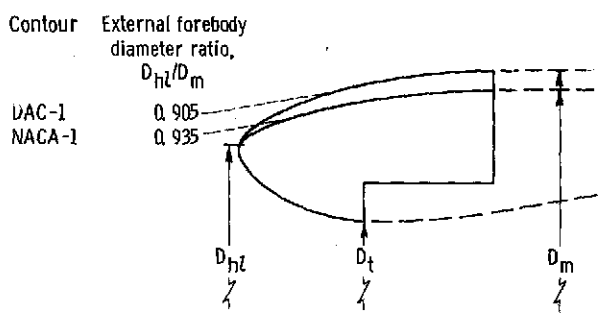

(c) External forebody diameter ratios. Internal lip contraction ratio, $(D_{hl}/D_t)^2$, 1.46.

Figure 4. - Entry-lip nomenclature and range of geometric variables tested.

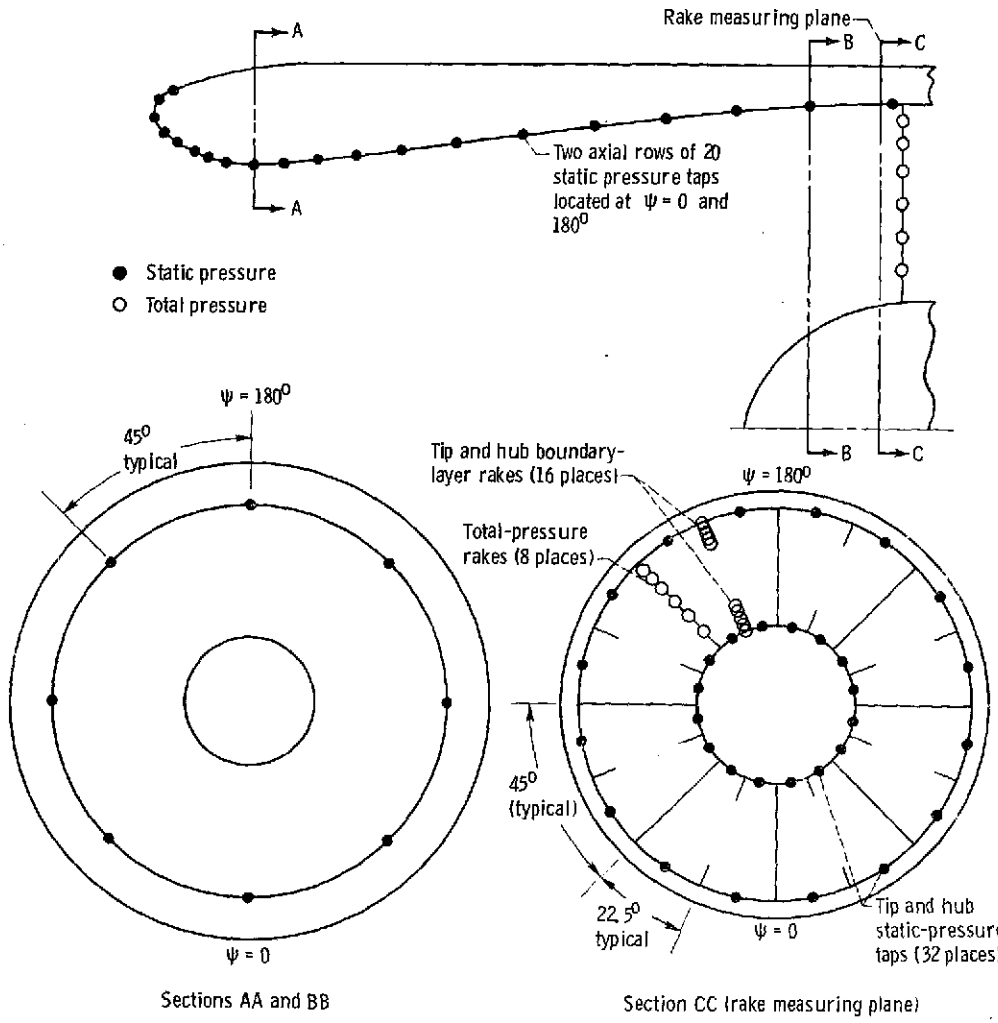

Figure 5. - Location of steady-state pressure instrumentation.

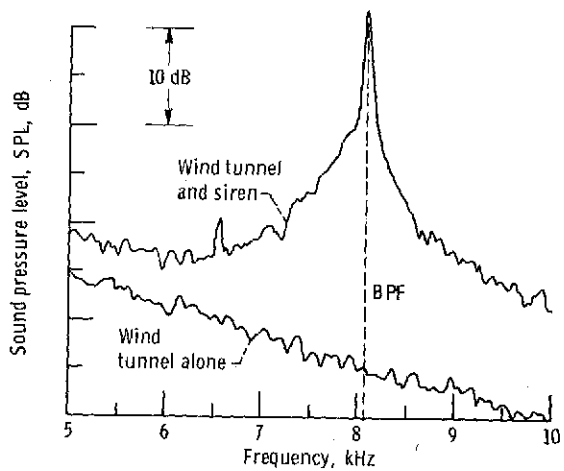

Figure 6. - Narrow band noise spectra showing characteristic of siren noise and wind tunnel noise. Inlet average throat Mach number, 0.6; free-stream velocity, 41 meters per second (80 knots).

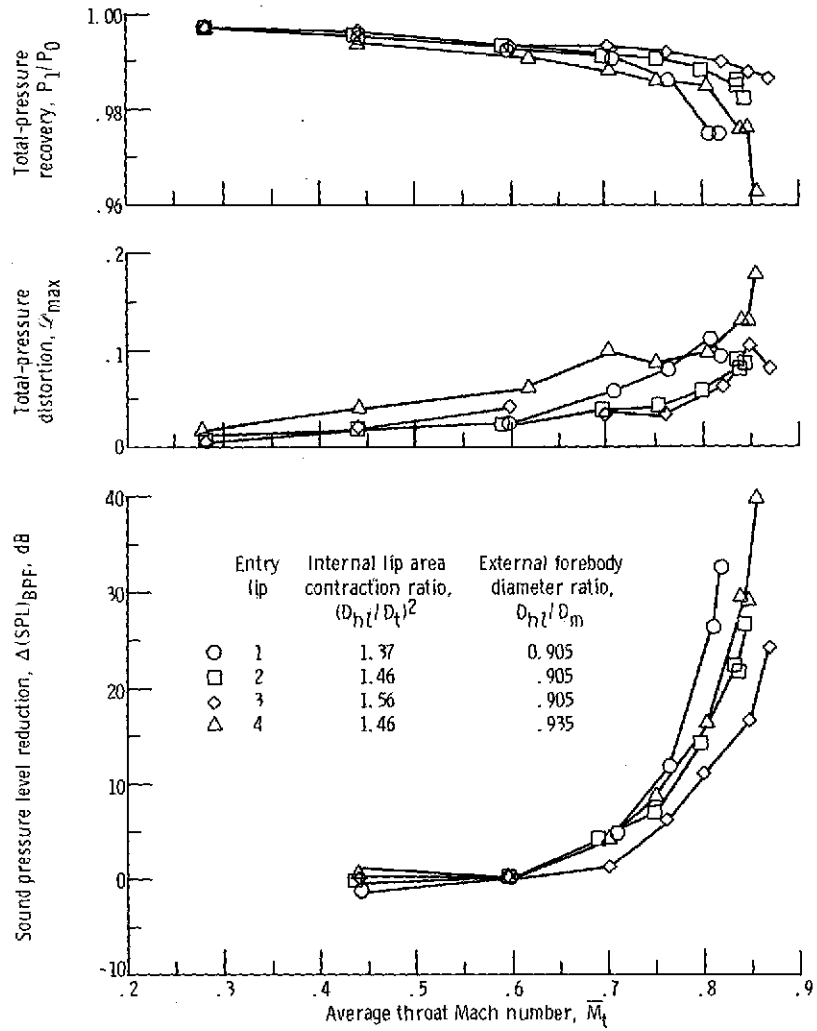

Figure 7. - Effect of entry-lip design and average throat Mach number on inlet aerodynamic and acoustic performances at static conditions.

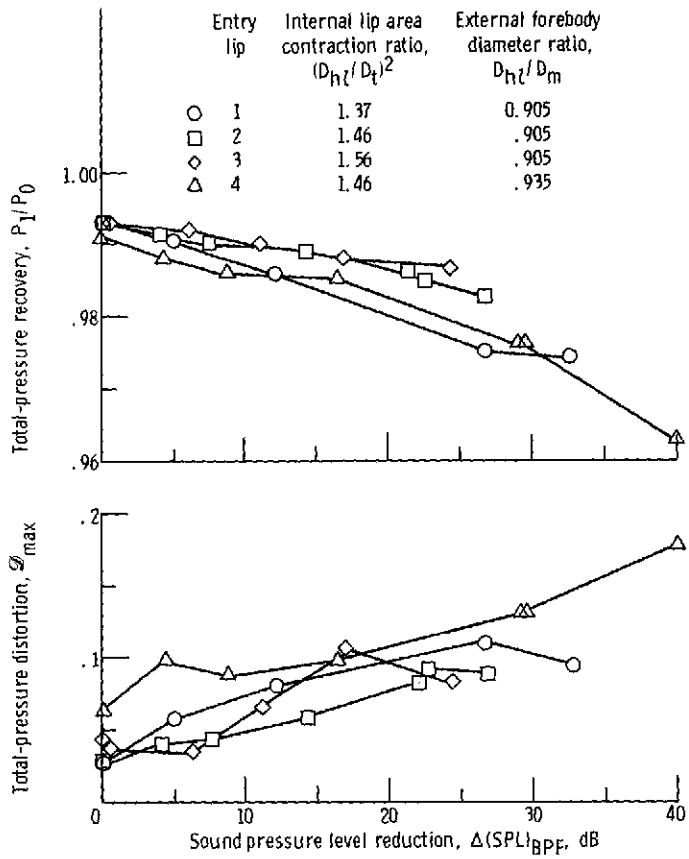

Figure 8. - Effect of entry-lip design on inlet aerodynamic and acoustic performances at static conditions.

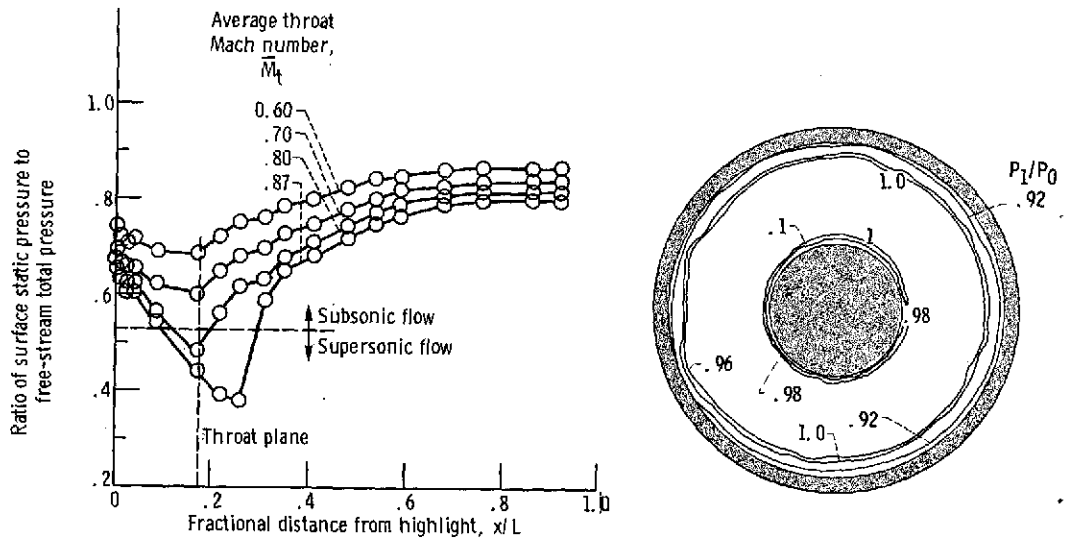

(a) Axial variation of surface static pressure as function of average throat Mach number.

(b) Total-pressure contours at rake measuring plane. Average throat Mach number, 0.87.

Figure 9. - Diffuser axial static-pressure distribution and rake plane total contours representative of those observed at static conditions. Entry lip 3; internal lip area contraction ratio, 1.56; external forebody diameter ratio, 0.905.

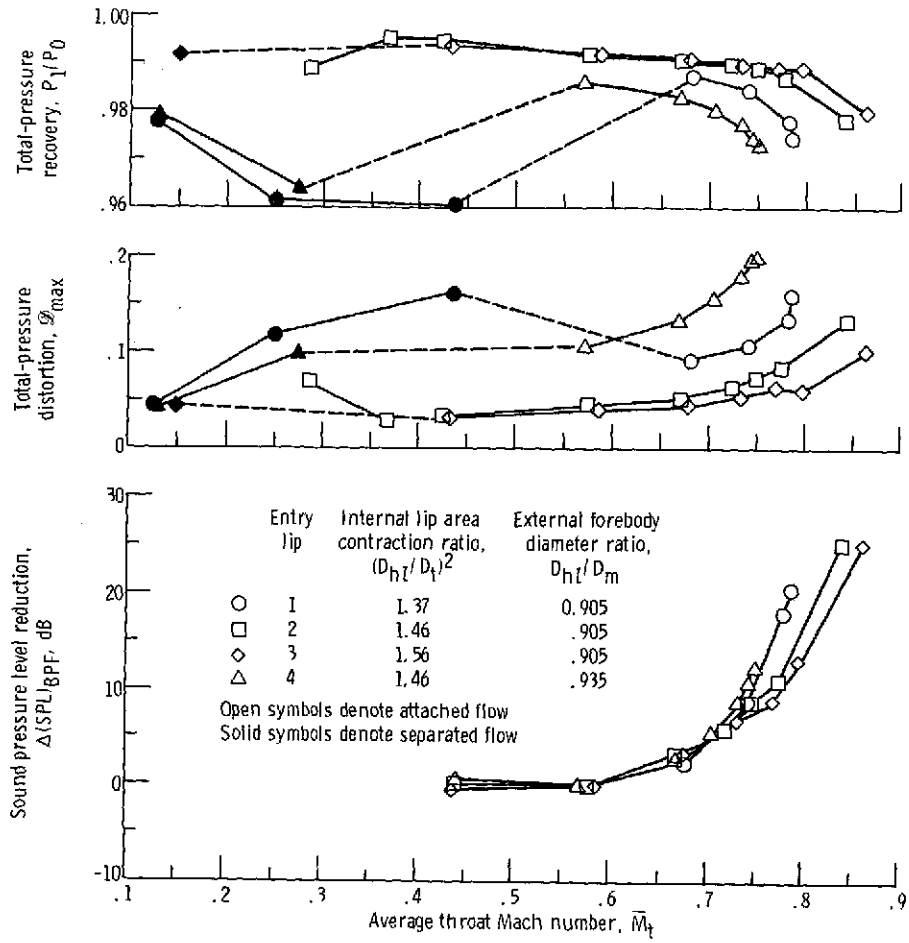

Figure 10. - Effect of entry-lip design and average throat Mach number on inlet aerodynamic and acoustic performances for crosswind condition. Free-stream velocity, 18 meters per second (35 knots); incidence angle, 90°.

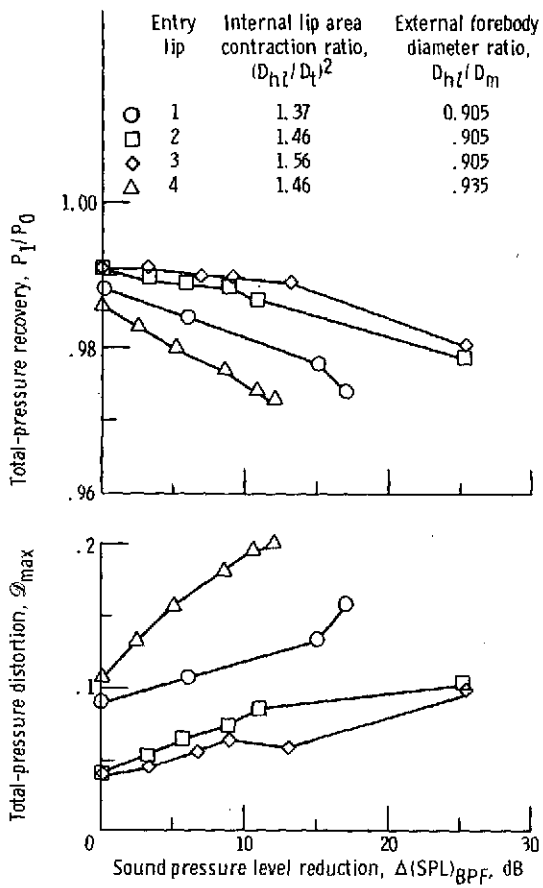

Figure 11. - Effect of entry-lip design on inlet aerodynamic and acoustic performances with crosswind. Free-stream velocity, 18 meters per second (35 knots); incidence angle, 90°; average throat Mach number, ≥0.6

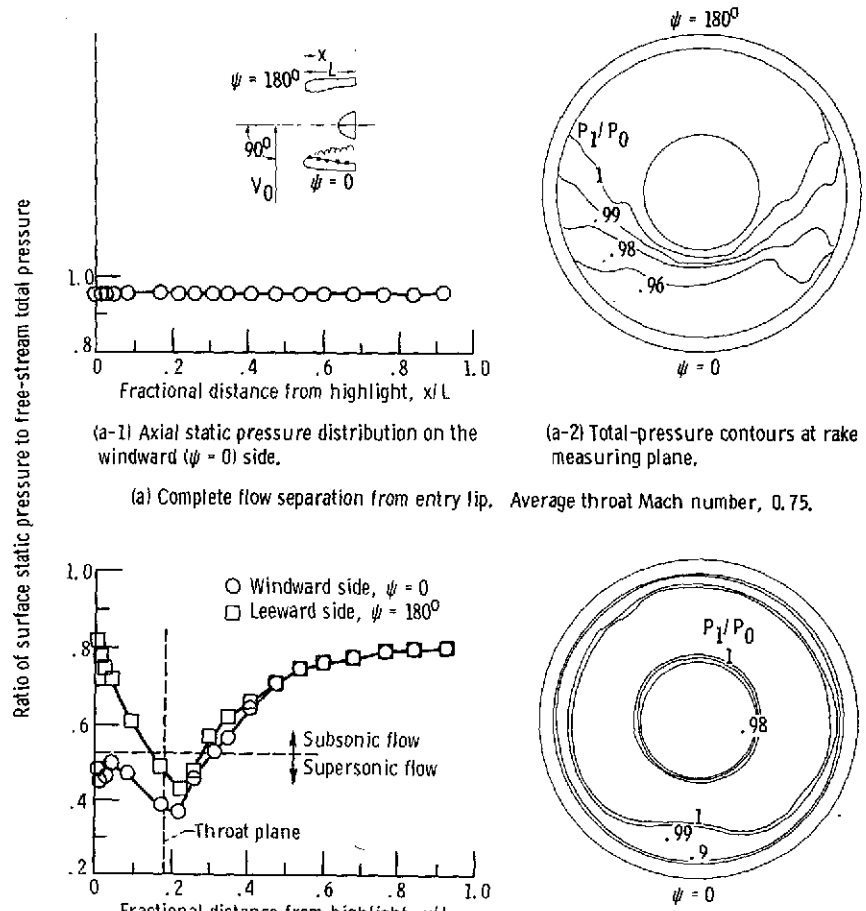

(a-1) Axial static pressure distribution on the windward ($\psi = 0$) side.

(a-2) Total-pressure contours at rake measuring plane.

(a) Complete flow separation from entry lip. Average throat Mach number, 0.75.

(b-1) Axial static pressure distribution.

(b-2) Total-pressure contours at rake measuring plane.

(b) Fully attached flow. Average throat Mach number, 0.86.

Figure 12. - Inlet axial static-pressure distributions and rake plane total-pressure contours representative of separation and attached flow conditions for crosswind condition. Free-stream velocity, 18 meters per second (35 knots); incidence angle, 90°; entry lip 3; internal lip area contraction ratio, 1.56; external forebody diameter ratio, 0.905.

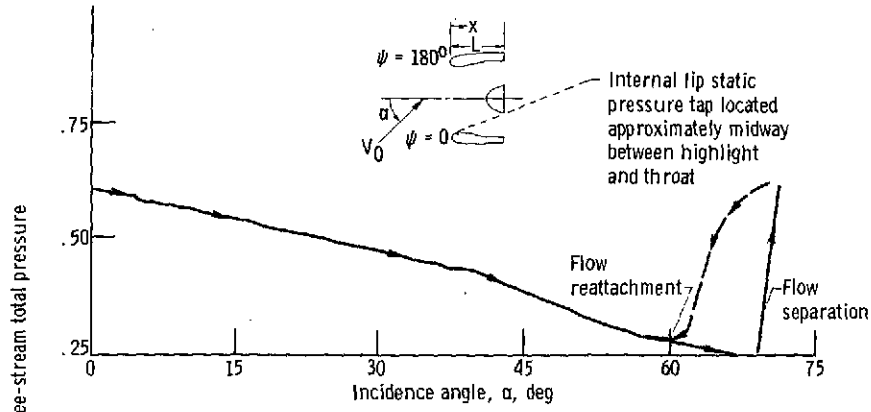

(a) Trace of internal lip static-pressure used to indicate incidence angle induced entry-lip flow separation and reattachment.

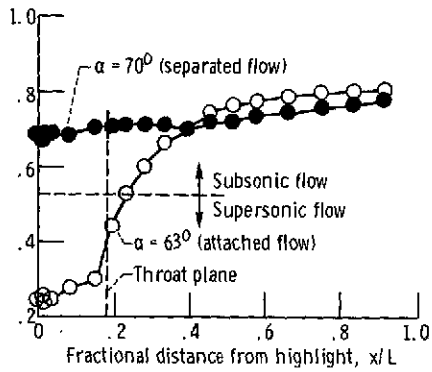

(b-1) Axial static pressure distribution on the windward (ψ = 0) side.

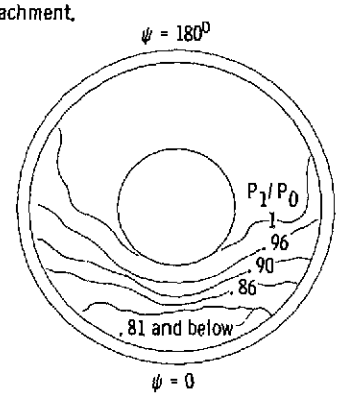

(b-2) Total-pressure contours at rake measuring plane resulting from entry lip flow separation. Incidence angle, 70°.

(b) Change in inlet axial static-pressure distribution produced by entry-lip flow separation and resulting total-pressure contours measured at rake plane.

Figure 13. - Representative static-pressure measurements and total-pressure contours used to indicate incidence angle induced entry-lip flow separation. Entry lip 2; free-stream velocity, 41 meters per second (80 knots).

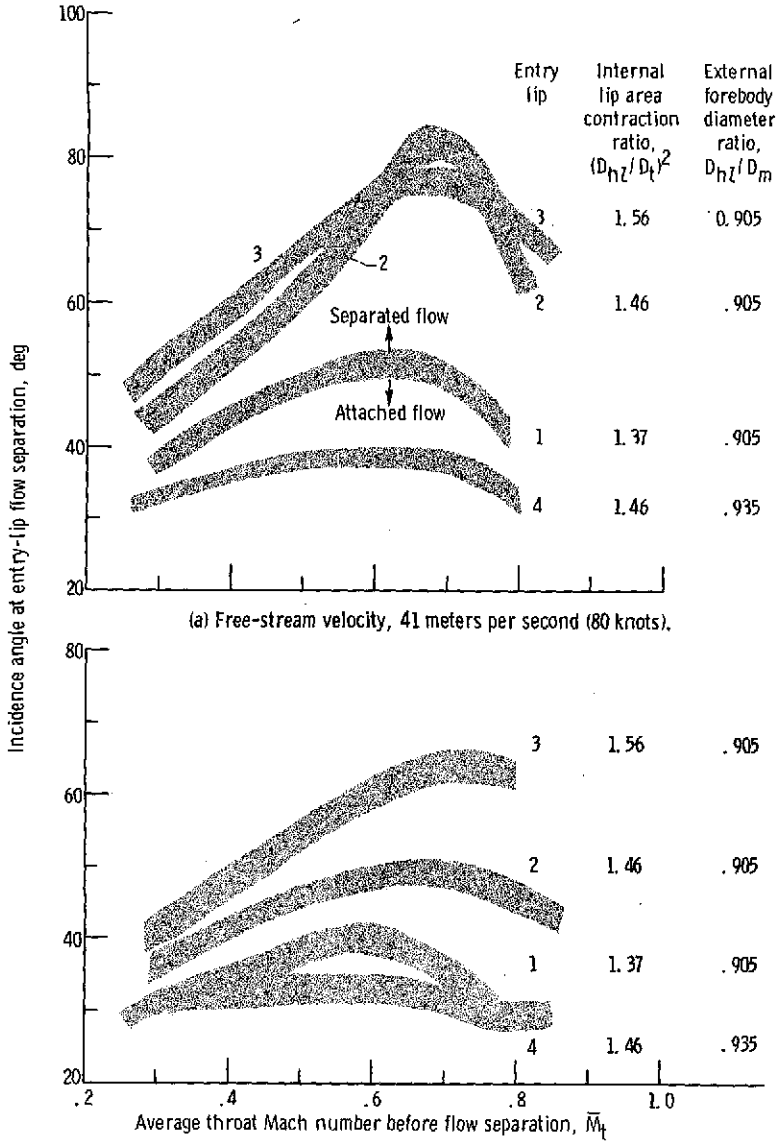

(a) Free-stream velocity, 41 meters per second (80 knots).

(b) Free-stream velocity, 61 meters per second (120 knots).

Figure 14. - Effect of entry-lip design and average throat Mach number on incidence angle at entry-lip flow separation. Data obtained by increasing incidence angle to point of flow separation.

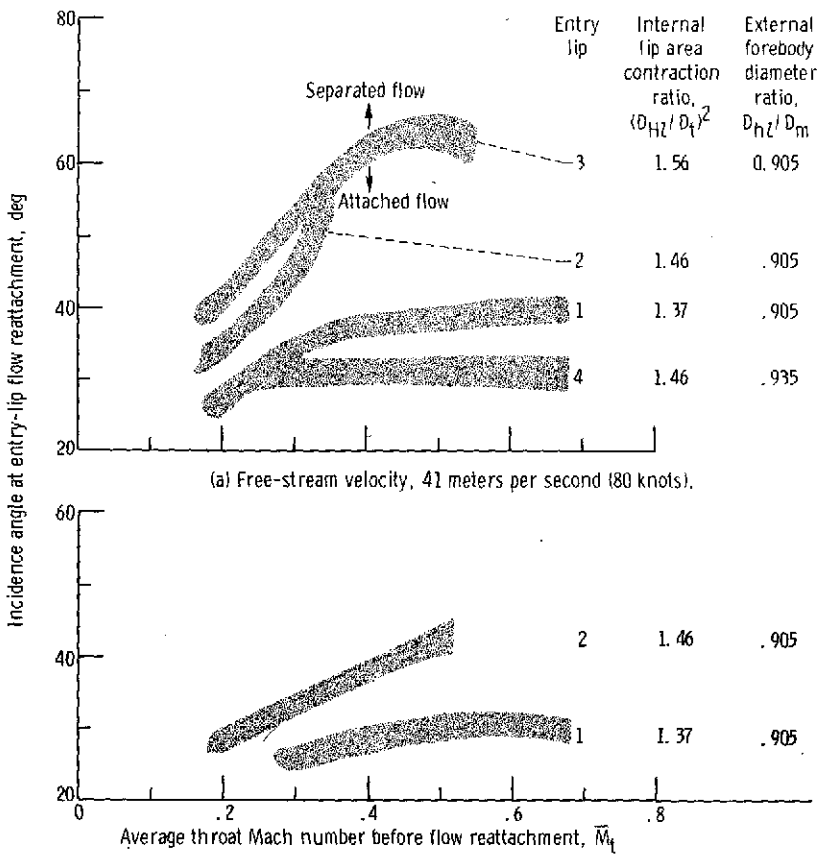

(a) Free-stream velocity, 41 meters per second (80 knots).

(b) Free-stream velocity, 61 meters per second (120 knots).

Figure 15. - Effect of entry-lip design and average throat Mach number on incidence angle at which entry-lip flow reattachment occurs. Data obtained by decreasing incidence angle to point of flow reattachment.

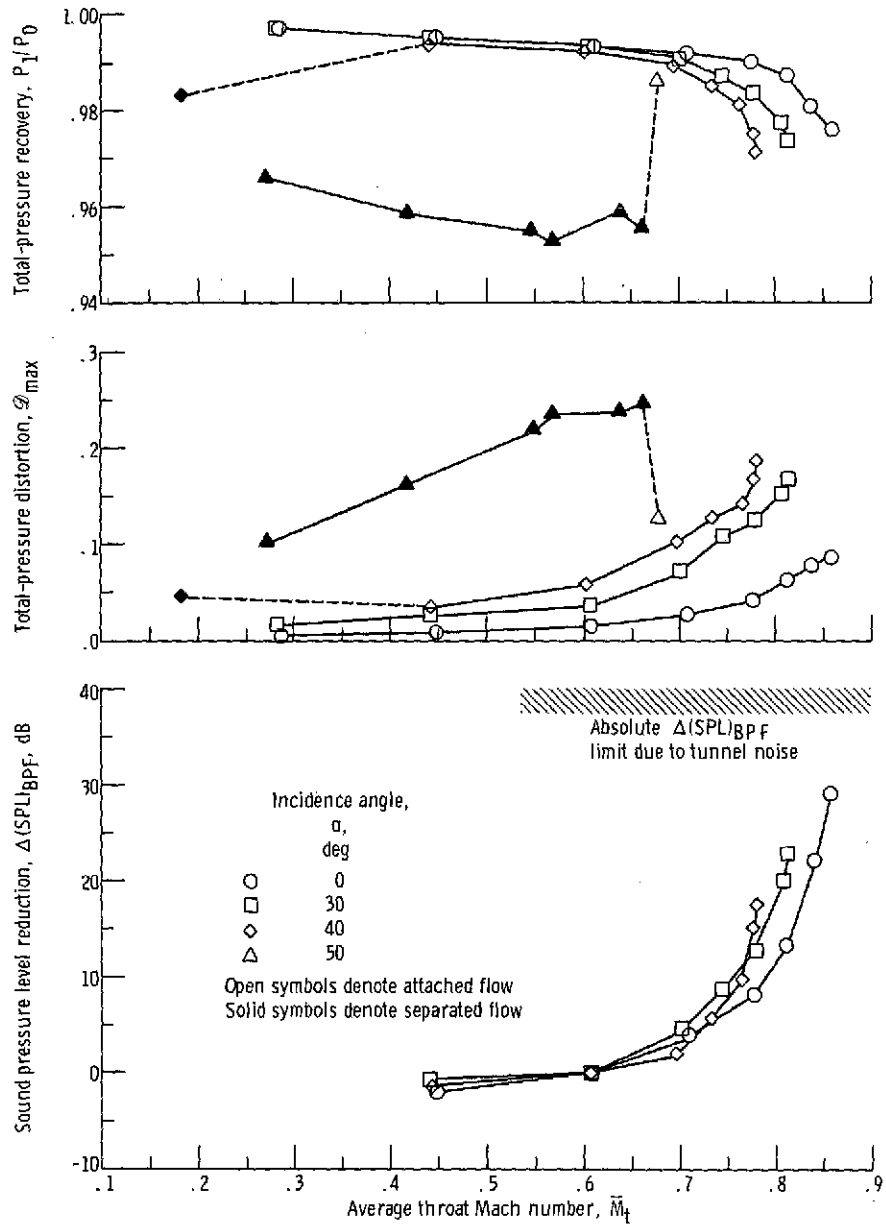

(a) Free-stream velocity, 61 meters per second (80 knots).

Figure 16. - Effect of incidence angle and average throat Mach number on aerodynamic and acoustic performances of entry lip 1. Internal lip area contraction ratio, 1.37; external forebody diameter ratio, 0.905.

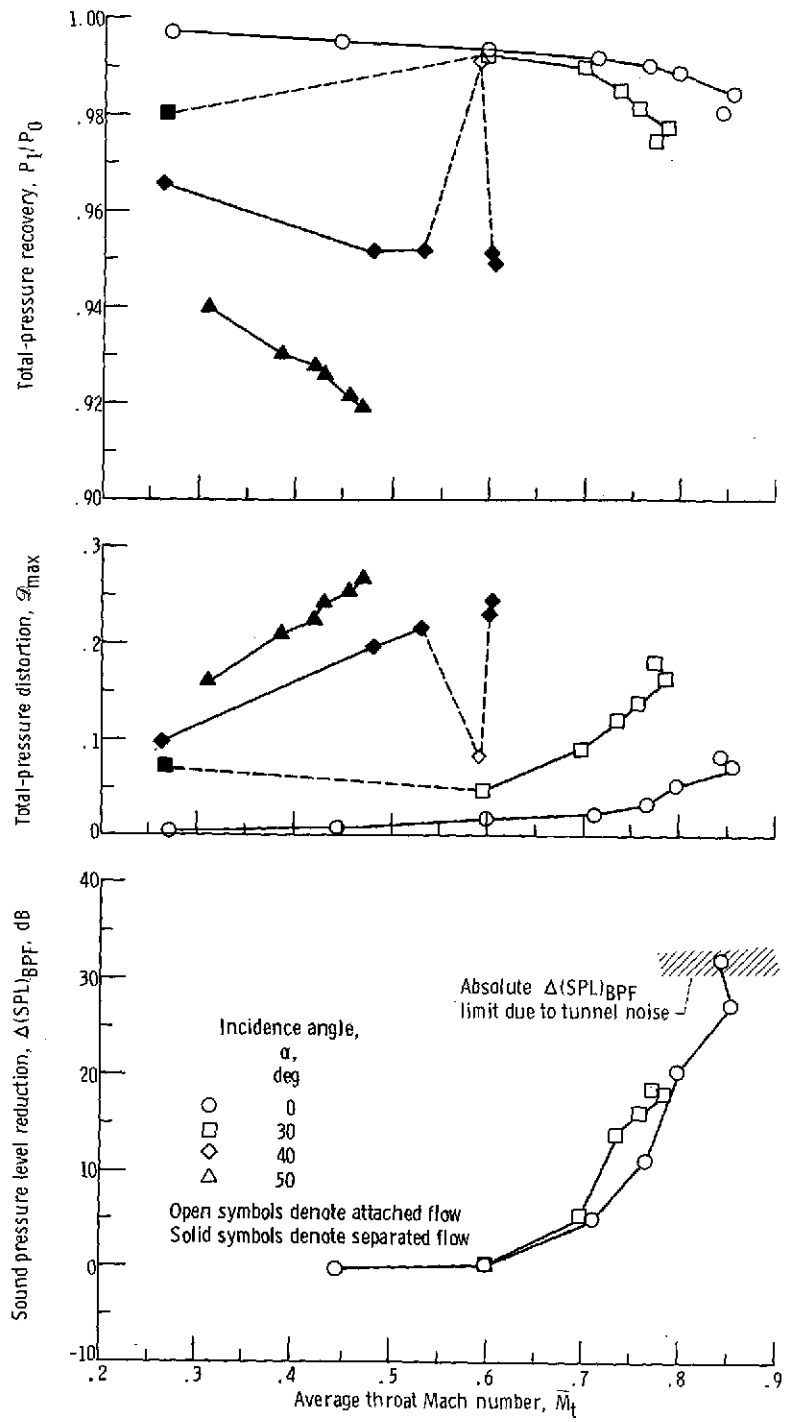

(b) Free-stream velocity, 61 meters per second (120 knots).

Figure 16. - Concluded.

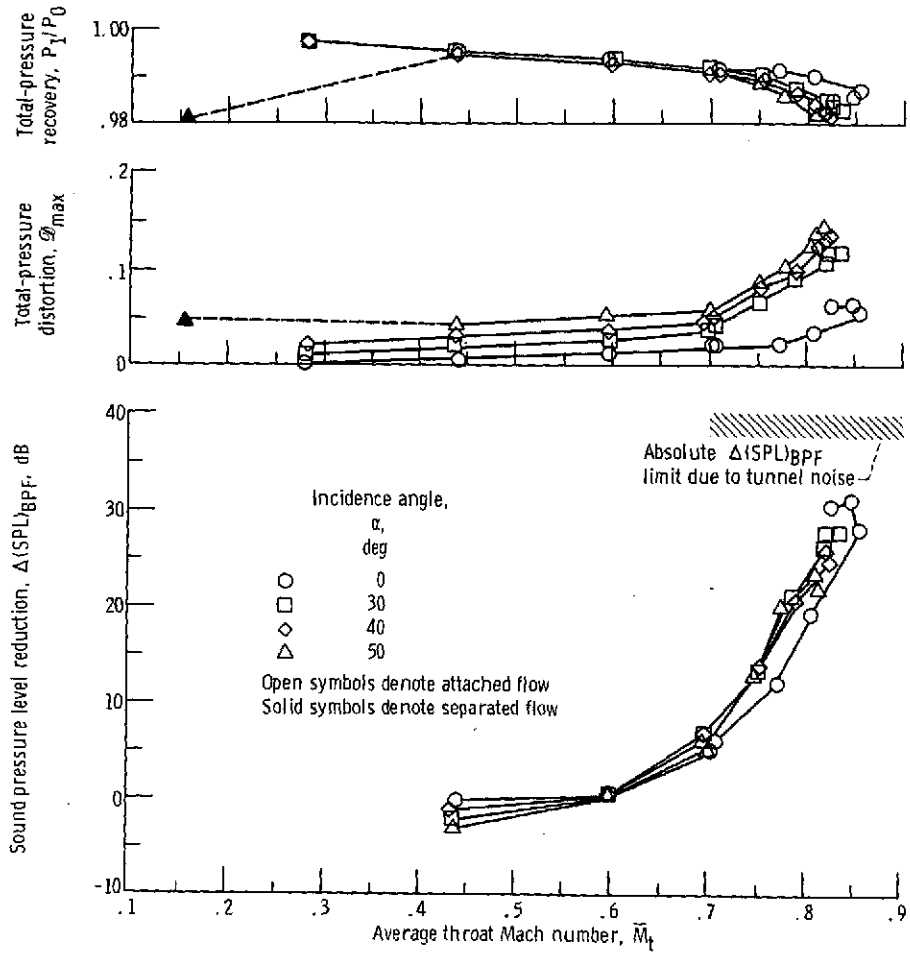

(a) Free-stream velocity, 41 meters per second (80 knots).

Figure 17. - Effect of incidence angle and average throat Mach number on aerodynamic and acoustic performances of entry lip 2. Internal lip area contraction ratio, 1.46; external forebody diameter ratio, 0.905.

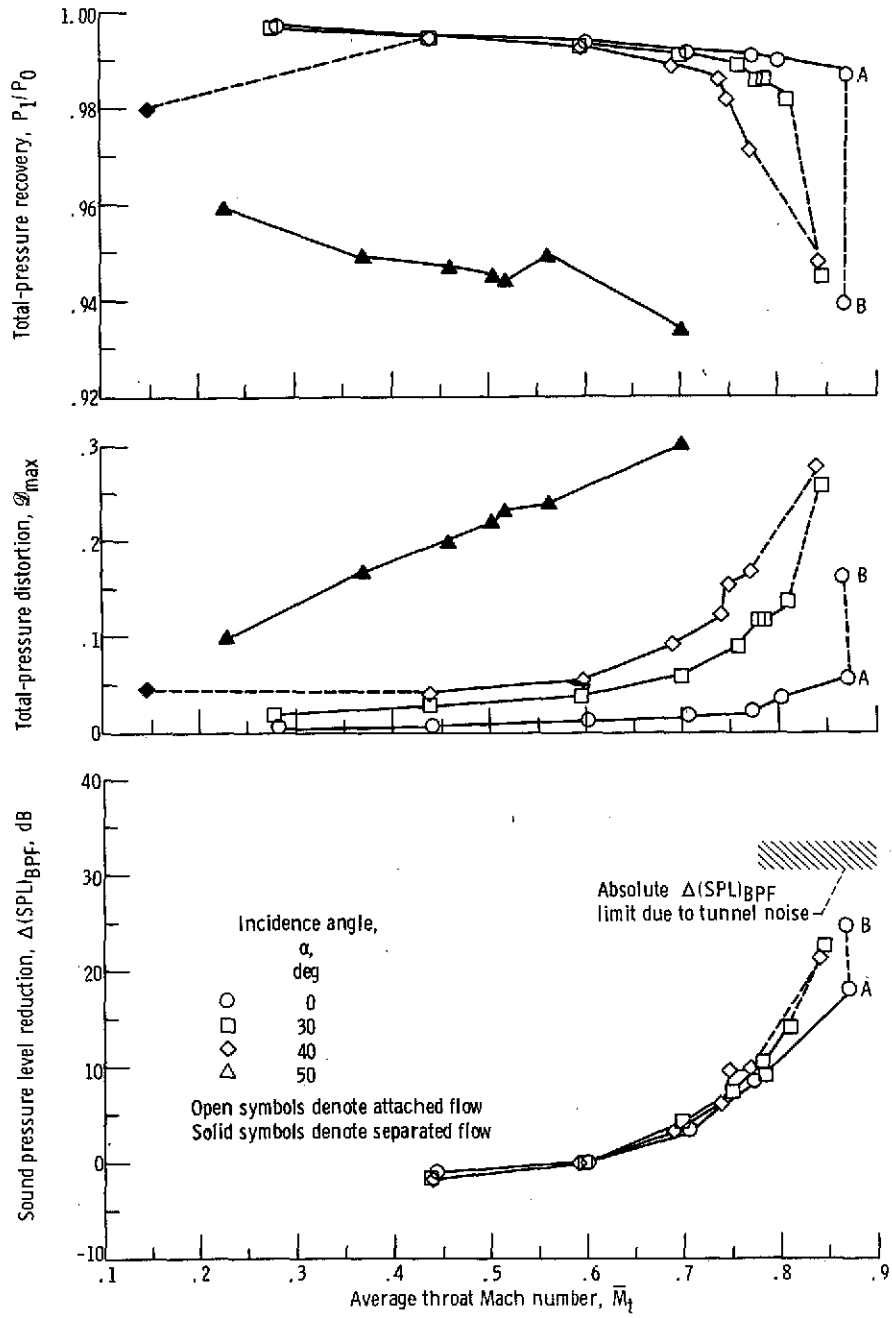

(b) Free-stream velocity, 61 meters per second (120 knots).

Figure 17. - Concluded.

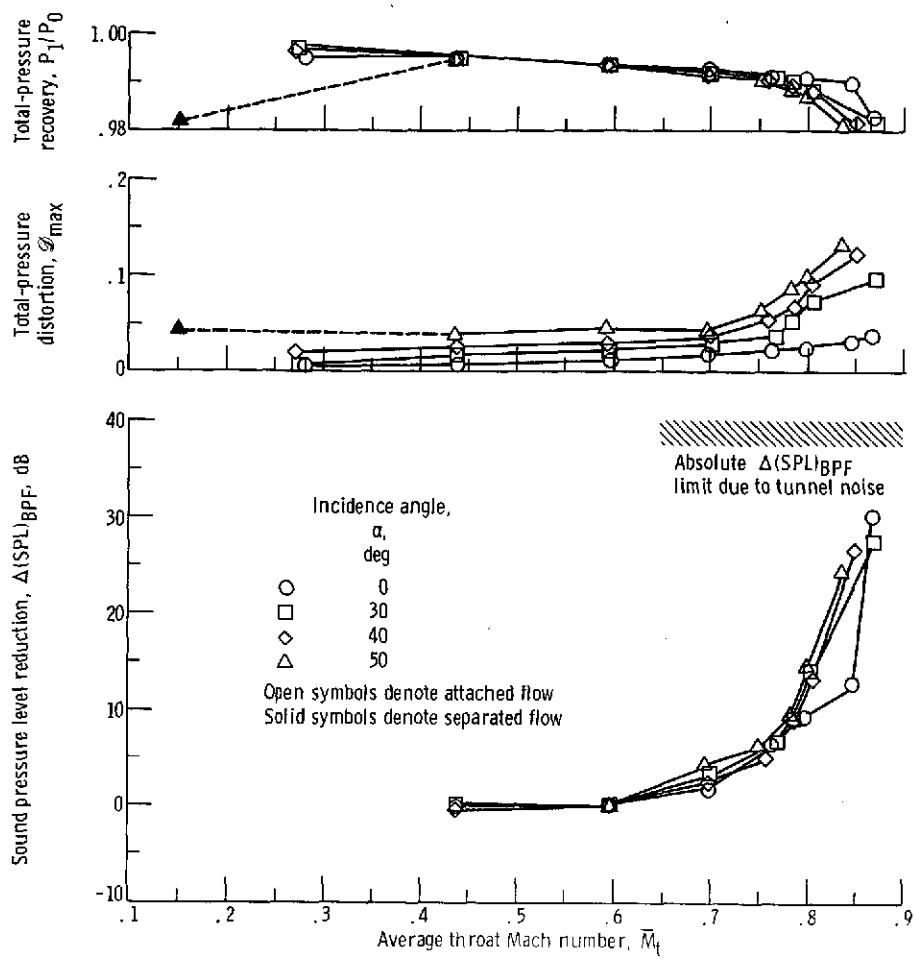

(a) Free-stream velocity, 41 meters per second (80 knots).

Figure 18. - Effect of incidence angle and average throat Mach number on aerodynamic and acoustic performances of entry lip 3. Internal lip area contraction ratio, 1.56; external forebody diameter ratio, 0.905.

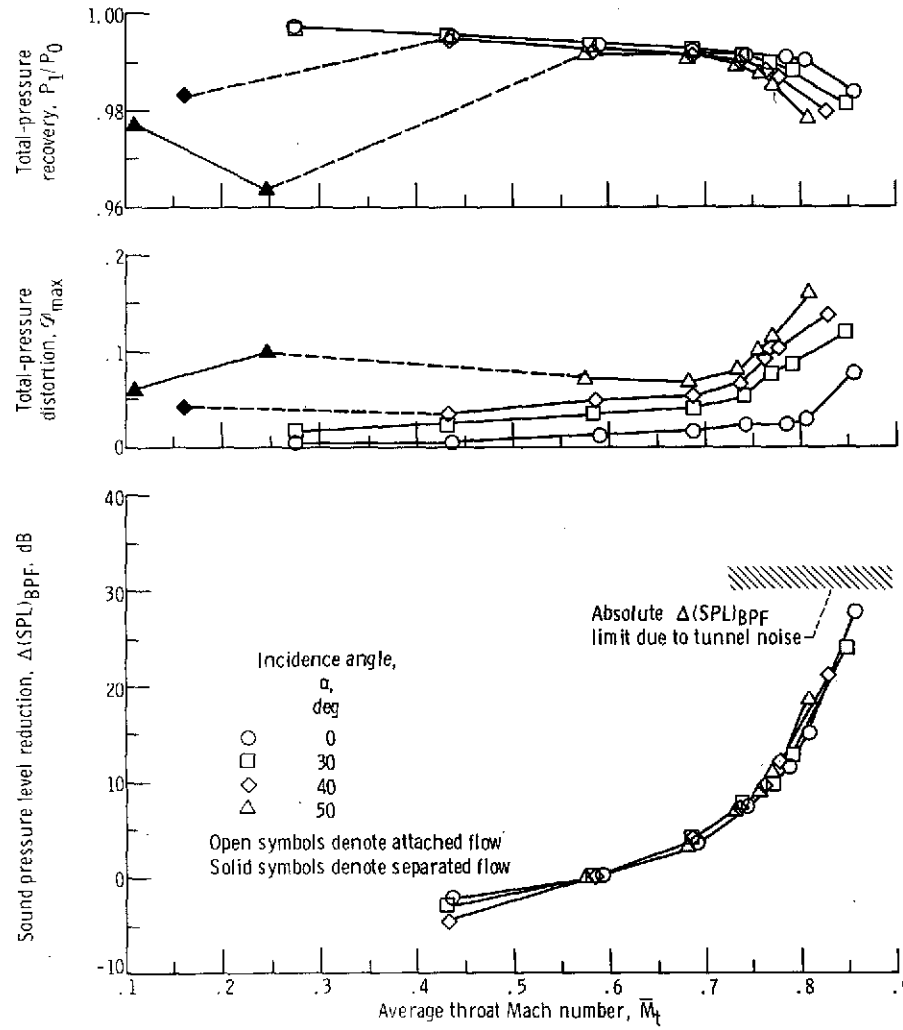

(b) Free-stream velocity, 61 meters per second (120 knots).

Figure 18. - Concluded.

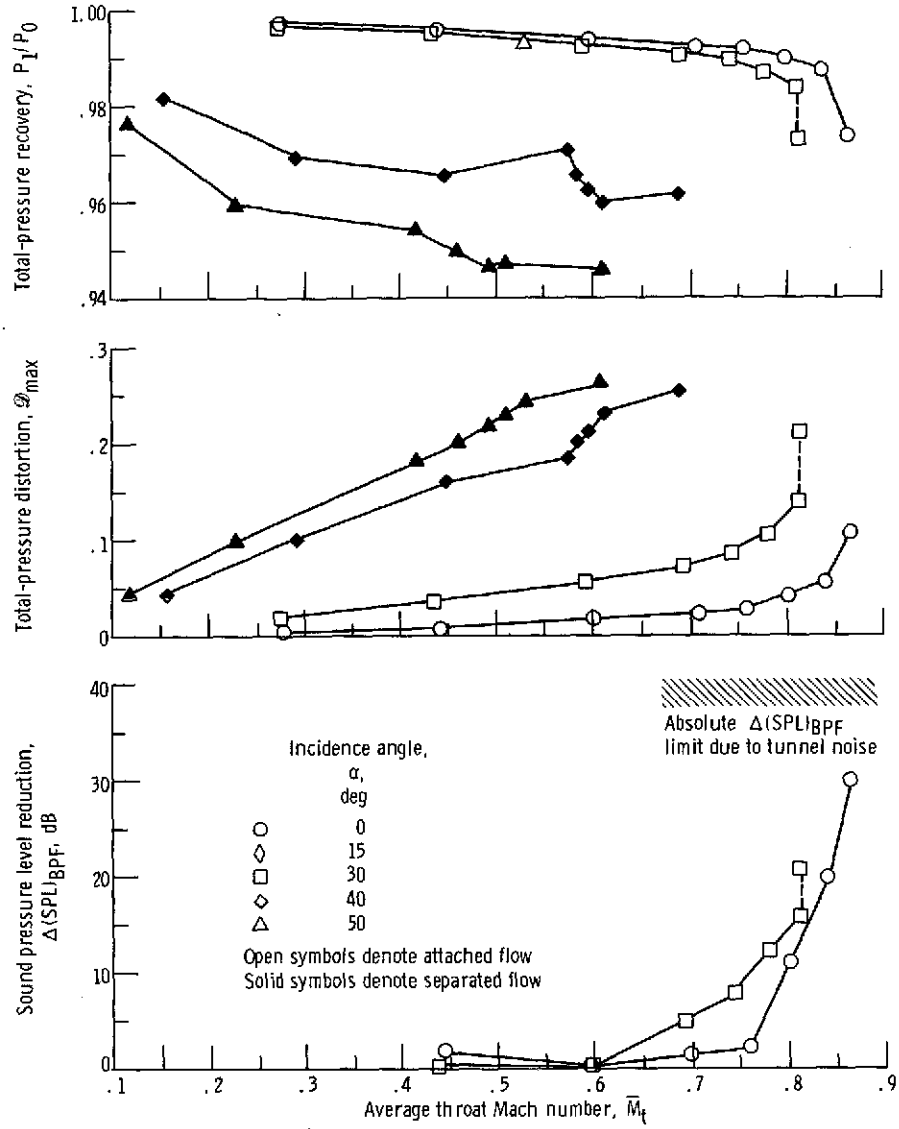

(a) Free-stream velocity, 41 meters per second (80 knots).

Figure 19. - Effect of incidence angle and average throat Mach number on aerodynamic and acoustic performances of entry lip 4. Internal lip area contraction ratio, 1.46; external forebody diameter ratio, 0.935.

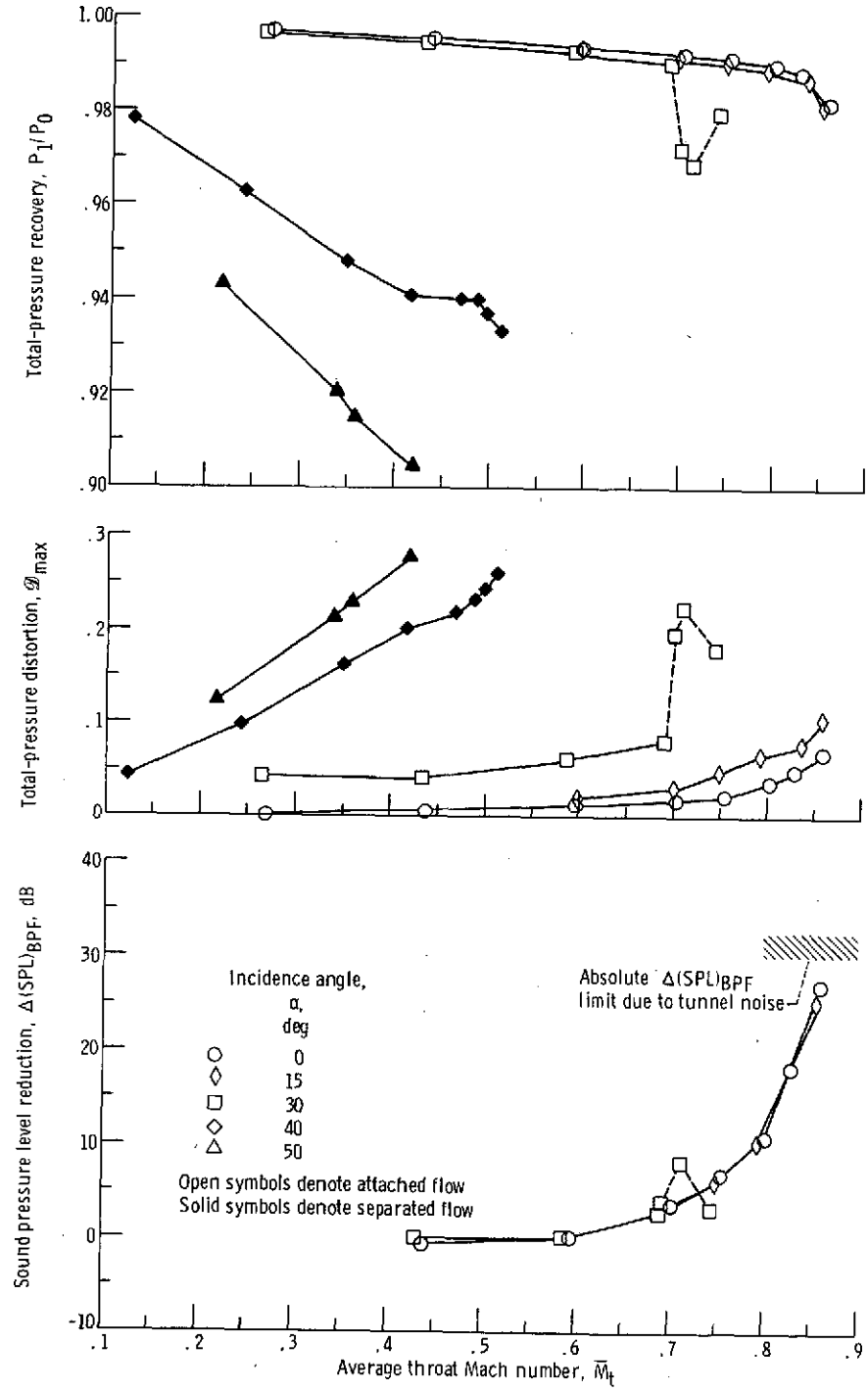

(b) Free-stream velocity, 61 meters per second (120 knots).

Figure 19. - Concluded.

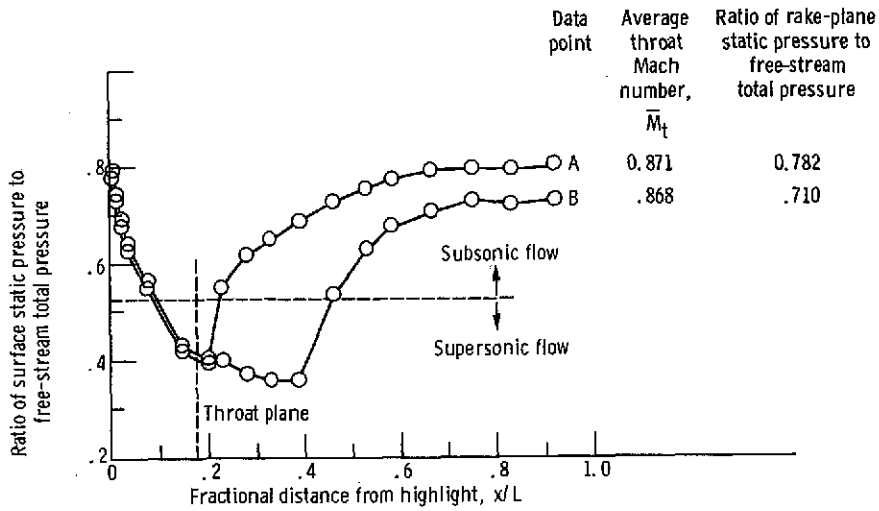

Figure 20. - Effect of reducing rake plane average static pressure on inlet axial static-pressure distribution. Entry lip 2; internal lip area contraction ratio, 1.46; external forebody diameter ratio, 0.905; free-stream velocity, 61 meters per second (120 knots); incidence angle, 0.

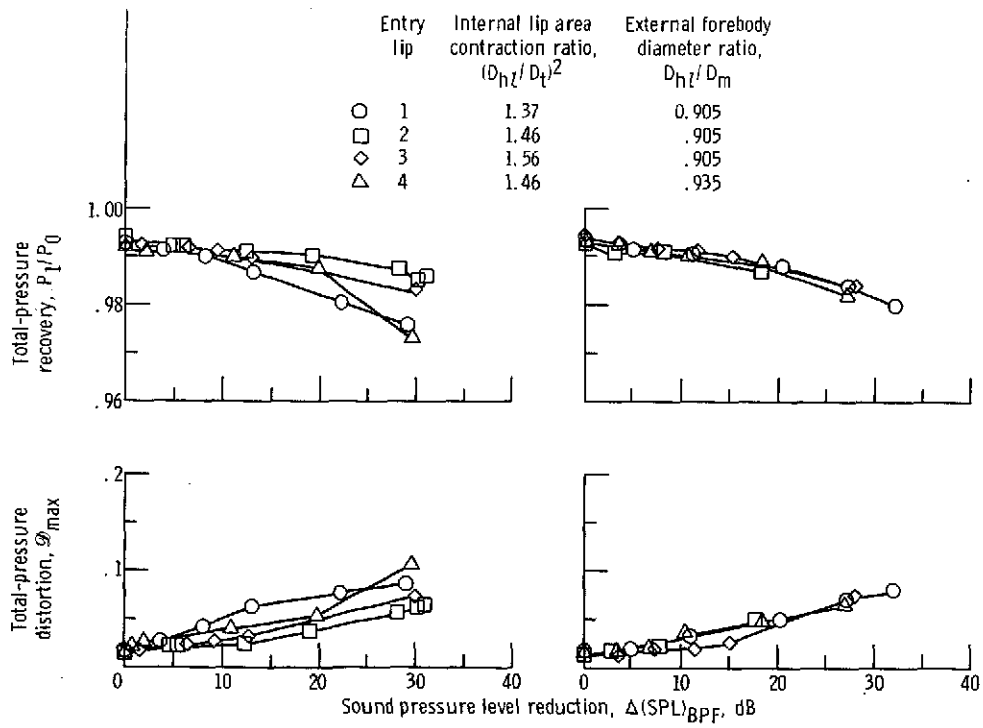

(a) Free-stream velocity, 41 meters per second (80 knots).

(b) Free-stream velocity, 61 meters per second (120 knots).

Figure 21. - Effect of entry-lip design on inlet aerodynamic and acoustic performances with attached flow. Incidence angle, 0; average throat Mach number, ≥ 0.6.

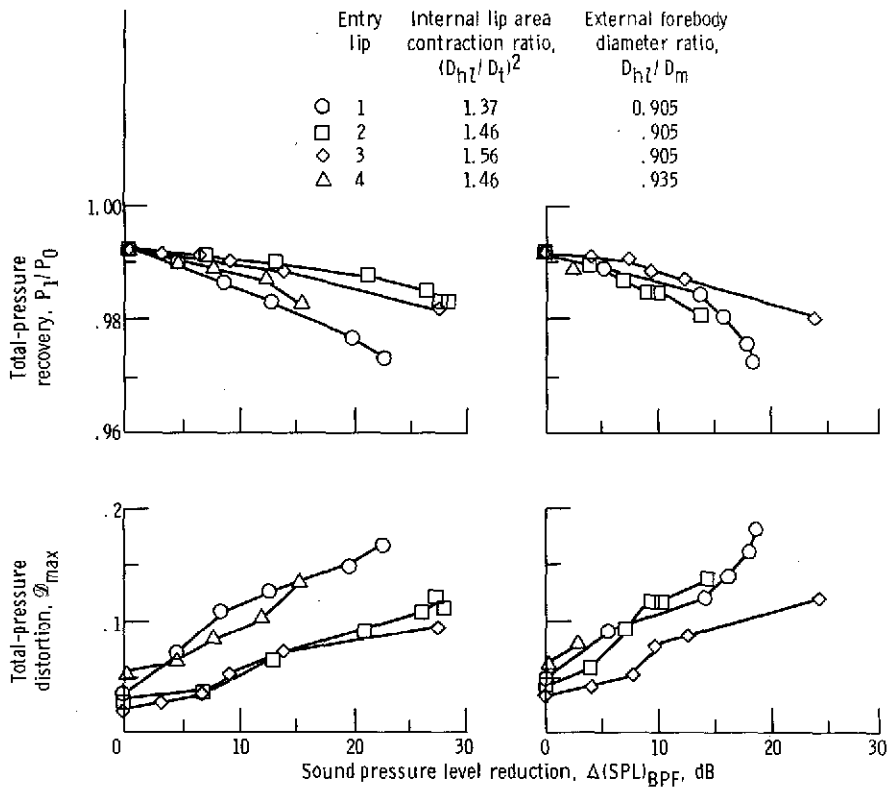

(a) Free-stream velocity, 41 meters per second (80 knots).

(b) Free-stream velocity, 61 meters per second (120 knots).

Figure 22. - Effect of entry-lip design on inlet aerodynamic and acoustic performances with attached flow. Incidence angle, 30°; average throat Mach number, $\geq$0.6.

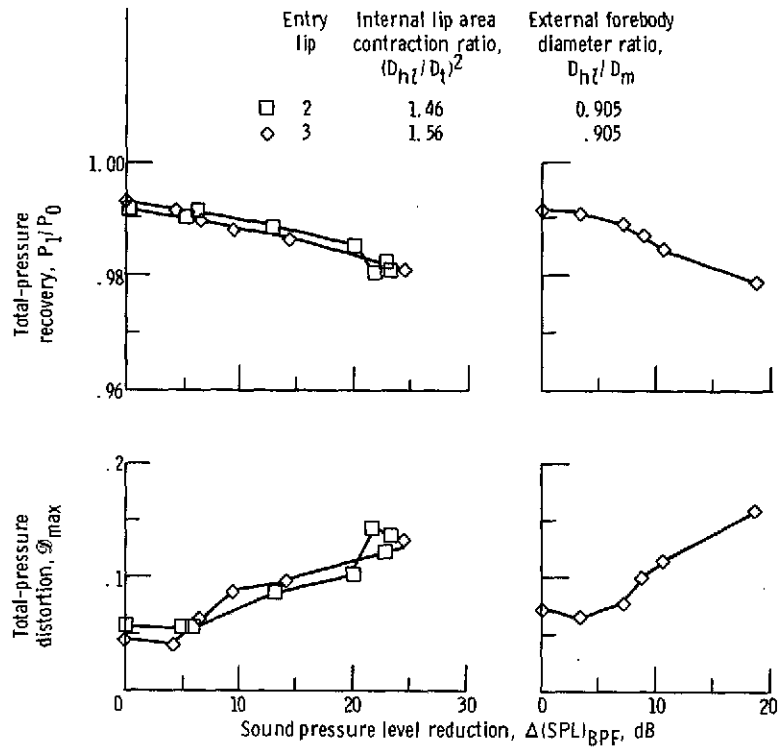

(a) Free-stream velocity, 41 meters per second (80 knots).

(b) Free-stream velocity, 61 meters per second (120 knots).

Figure 23. - Effect of entry-lip design on inlet aerodynamic and acoustic performances with attached flow. Incidence angle, 50^0; average throat Mach number, ≥ 0.6.

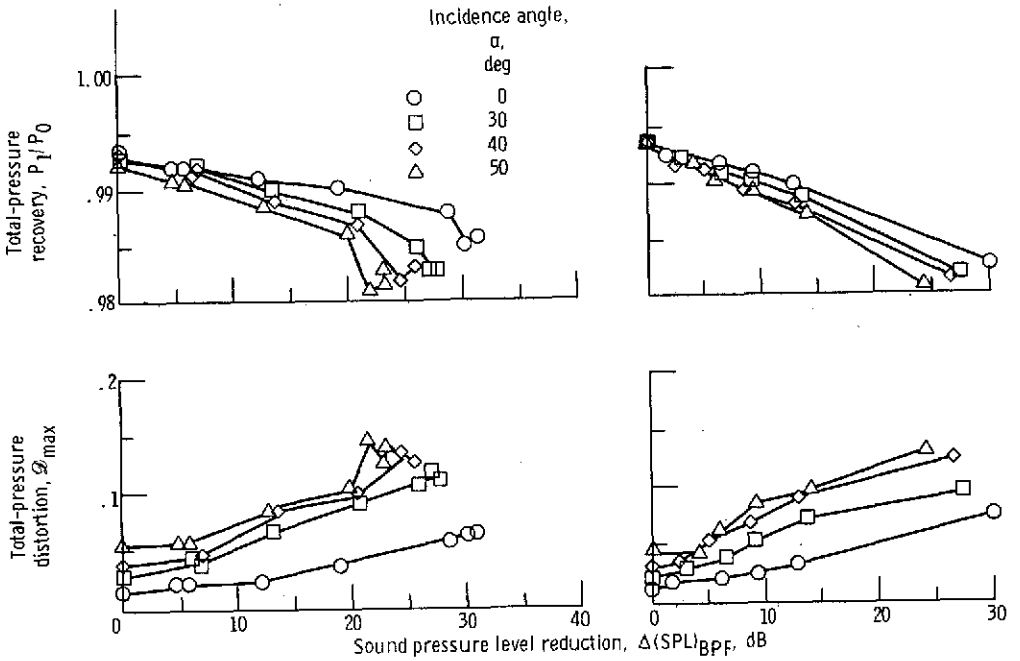

(a) Entry lip 2; internal lip contraction ratio, 1.46; external forebody diameter ratio, 0.905.

(b) Entry lip 3; internal lip area contraction ratio, 1.56; external forebody diameter ratio, 0.905.

Figure 24. - Effect of incidence angle on inlet aerodynamic and acoustic performances with attached flow. Free-stream velocity, 41 meters per second (80 knots); average throat Mach number, ≥ 0.6.

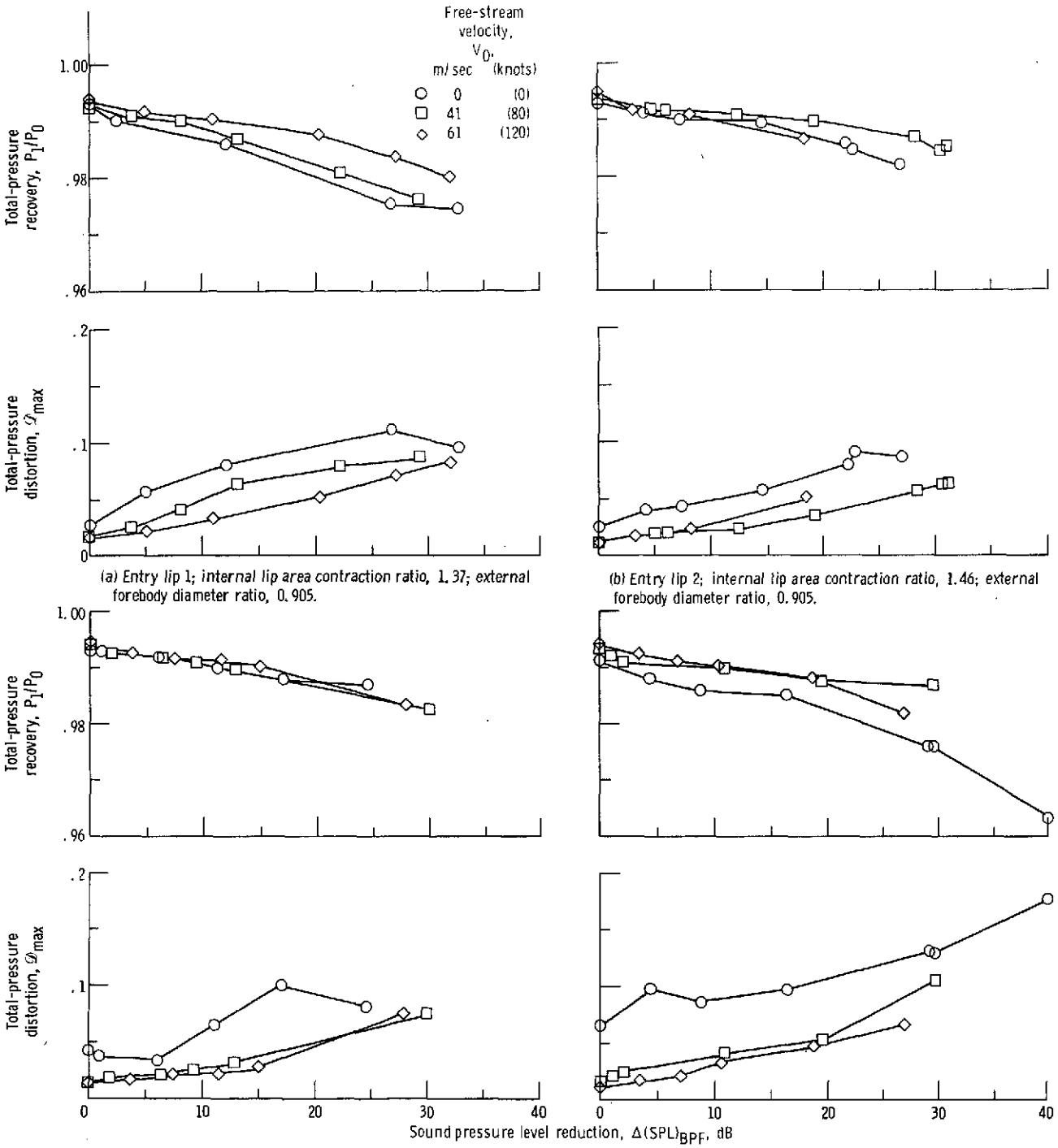

(a) Entry lip 1; internal lip area contraction ratio, 1.37; external forebody diameter ratio, 0.905.

(b) Entry lip 2; internal lip area contraction ratio, 1.46; external forebody diameter ratio, 0.905.

(c) Entry lip 3; internal lip contraction ratio, 1.56; external forebody diameter ratio, 0.905.

(d) Entry lip 4; internal lip area contraction ratio, 1.46; external forebody diameter ratio, 0.935.

Figure 25. - Effect of free-stream velocity on inlet aerodynamic and acoustic performances with attached flow. Incidence angle, 0°; average throat Mach number, ≥ 0.6.

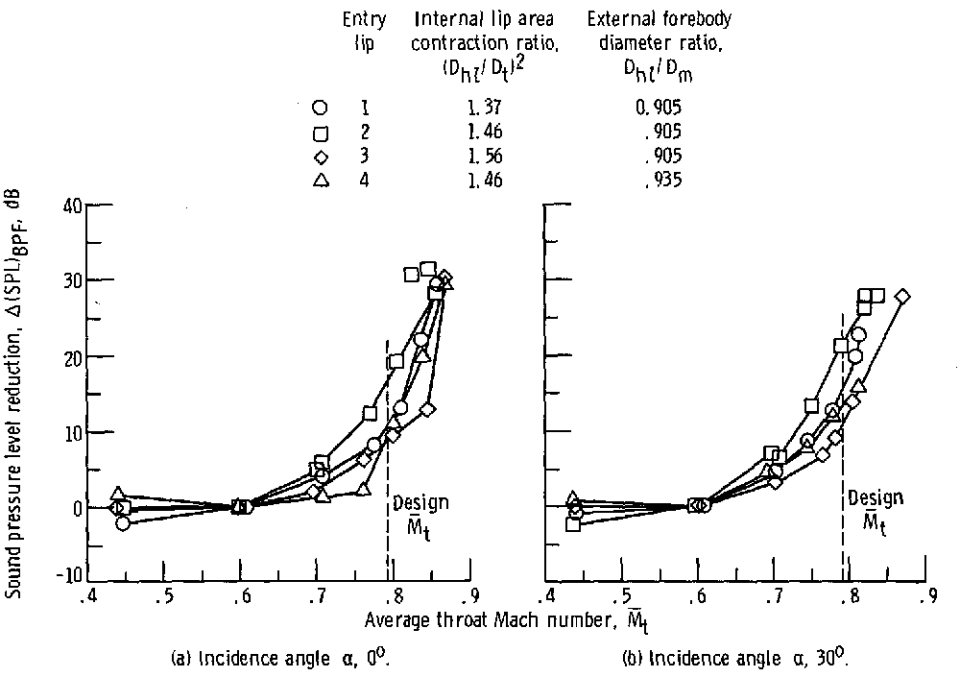

Figure 26. - Effect of average throat Mach number on sound pressure level reduction. Free-stream velocity, 41 meters per second (80 knots).